

A Study of 3D Femoral Rotational Effects on X-ray Femoral Shapes Using Statistical Shape Modelling

by

Casper Donkervoort

to obtain the degree of Master of Science
at the Delft University of Technology,
to be defended publicly on the 28th of August 2024

Student Name	Student Number
Casper Donkervoort	4319516

Thesis Committee:

Supervisor
Committee member
Committee member

Dr. ir. N. Tümer
Dr. R. Agricola
Prof. dr. ir. H.H. Weinans

TU Delft
Erasmus MC
UMC Utrecht

An electronic version of this thesis is available at <http://repository.tudelft.nl/>.



Summary

This thesis explores the impact of 3D femoral rotational effects on 2D X-ray femoral shapes using Statistical Shape Modeling (SSM). The study is driven by the clinical relevance of accurately diagnosing hip disorders from 2D radiographs, which are inherently influenced by the femur's position and rotation. The primary objective is to understand how these rotations affect the femur's apparent shape on radiographs and quantify the influence of rotation on shape variations observed in 2D SSMs.

The research was structured around two main experiments. The first experiment involves the creation of a 3D SSM of the whole femur using CT scans. This model was then used to explore how projections of the proximal femur change with different rotations. The second experiment focuses on the proximal femur and constructs two 2D SSMs. These were derived from Digitally Reconstructed Radiographs (DRRs) of the proximal femur, which are obtained by rotating the CTs ($\pm 30^\circ$ in 5° increments) around the shaft axis of the femur. One 2D SSM is based solely on DRR data, while the other combines DRR data with the WorldCOACH dataset of hip X-rays. This approach aims to provide an understanding of how rotation influences the shape modes of the femur as described by the 2D SSMs. For the first five shape modes the resulting b -values presented in a boxplot. Lastly, Welch's Analysis of Variance (ANOVA) is performed on these b -values for both 2D SSMs. The ANOVA analysis is performed on the following independent values: the femur, which represents the natural bone shape of that specific femur, and the angle, which represents the angle of rotation at which the DRR was created.

Findings show that sensitivity to angle changes varies across SSM modes, with shape changes due to external rotation being more evident than those caused by internal rotation. The combined results from the plots and Welch's ANOVA analyses of the two models (DRR-only and combined WorldCOACH and DRR) indicate that modes 1 to 4 are more heavily influenced by rotation, while mode 5 is more influenced by natural shape differences. This suggests that higher modes, which describe more specific and less variable shapes, are less influenced by rotation and more by intrinsic anatomical variations.

Nomenclature

Abbreviations

Abbreviation	Definition
ANOVA	Analysis of Variance
AP	Anteroposterior
CT	Computed Tomography
DRR	Digitally Reconstructed Radiograph
OA	Osteoarthritis
PCA	Principal Component Analysis
SAM	Statistical Appearance Model
SSM	Statistical Shape Model

Contents

Summary	i
Nomenclature	ii
Abbreviations	ii
Contents	iii
1 Introduction	1
2 Methods	2
2.1 Basics of Statistical Shape Modelling (SSM)	3
2.2 Datasets	4
2.3 Experiment 1: 3D SSM of the femur and its 2D projection	5
2.3.1 From full-body CT to segmented femur	5
2.3.2 Creating landmarks and correspondence in 3D	6
2.4 Experiment 2: Digitally Reconstructed Radiographs (DRRs) and 2D SSMs	8
2.4.1 Creation of DRRs	8
2.4.2 Creating contours	8
2.4.3 Creating Landmarks on the DRRs	8
2.4.4 Creation of 2D SSMs	9
2.4.5 Analysis of the resulting b -values	9
3 Results	10
3.1 Experiment 1: 3D SSM of the femur and its 2D projection	11
3.1.1 3D Femoral SSM	11
3.1.2 2D plots of 3D modes	14
3.2 Experiment 2: Digitally Reconstructed Radiographs (DRRs) and 2D SSMs	16
3.2.1 DRRs	16
3.2.2 2D SSMs: Shape modes	16
3.2.3 b -values: Boxplots	21
3.2.4 b -values: Individual Curves	23
3.2.5 b -values: Welch's ANOVA	26
4 Discussion	27
5 Conclusion	31
Bibliography	32
A Protocol Proximal Femur SSM points	36
A.1 Lesser trochanter	36
A.2 Rest of proximal femur	36
A.3 Greater trochanter, posterior part	36
A.4 Curve model (with new landmarks incorporated):	37
A.5 General rules:	37

B Shape modes of WorldCOACH	37
C Boxplots: zoomed in	38
D Curves of tracked bones in Projected 2D SSM	40
E Statistical Appearance models	41

1

Introduction

A two-dimensional radiograph is a projection-based imaging method that is often used for diagnosing hip disorders. As this technique is projection-based, the projection shapes are influenced by the position and rotation of the subject. Changes in the appearance of the femur due to changes in position or rotation of the femur have been shown in previous studies. Characteristics such as joint space width between femur and pelvis, length of the anatomical femur axis, femoral neck/head shape, lesser trochanter size, and bone mineral density can appear different in 2D plane when the femur is in a different position or rotation [1], [2], [3], [4].

The clinical relevance of the apparent shape becomes clear when hip shapes are used to predict or diagnose diseases such as Osteoarthritis (OA) or hip dysplasia [5], [6], [7]. In these studies, 2D and 3D statistical shape models (SSM) were used to analyse different proximal femur and hemipelvis shapes. SSMs are a statistical model that describes the average shape distribution and the main shape modes within a population [8]. In Van Buuren et al., it was already concluded that some hip shape features, like cam morphology (femoroacetabular impingement), are associated with hip OA. Also, some feature combinations increase the risk of hip OA [7]. Another study used an SSM to analyse a dataset of hip dual-energy X-ray absorptiometry (DXA) scans of men aged 65 and older, finding associations between larger lesser trochanters, cam morphology, and a higher prevalence of radiographic hip OA [9].

Given that 2D apparent shapes are used for prediction, diagnosis, and analysis, understanding the extent of shape differences between the projected apparent shape and the actual shape used for analysis is crucial. More specifically, it is essential to determine which shape features are less influenced by the position and rotation of the femur in projection images. In Waarsing et al., it was already mentioned that some shape modes might reflect the effect of internal and external rotation on the projected femur [10]. This study suggests that an increased anteversion angle or a limitation in the internal rotation due to pain, commonly observed in osteoarthritis (OA) patients, could be potential explanations for the observed femoral shape changes.

Previous research has explored methods to correct the projected shape to the actual desired shape. One study corrected the femoral offset appearance on a radiograph using a mathematical non-linear correlation between femur rotation and projected femoral offset [11]. However, this method relied on implants in the femur, which does not apply to all patients. Some other methods have been developed to assess the rotation of the femur when a bilateral radiograph is available as information. This includes methods such as inspecting the size of the lesser trochanter and comparing the lesser trochanters on contralateral sides [12], [13]. A downside of such a technique is that more than one radiograph is needed to create a good guess for the rotation.

A more advanced technique has been developed to eliminate the need for multiple radiographs or the inclusion of the contralateral bone in the radiograph. This method integrates a statistical shape and appearance model (SSAM) with machine learning techniques to accurately estimate rotation from a single-view radiograph [14]. Like SSMs describe the shape, statistical appearance models (SAM) are types of statistical models that describe the average density distribution together with the main modes of variation of density distribution within a population [8]. When a SSM and SAM are combined, they form a SSAM.

The role of the SSAM in the study of Väänänen et al. [14] was to simulate artificial population bones to train a linear regression model and a deep learning model to estimate the rotation of a proximal femur in a projection image. Despite demonstrating the feasibility of estimating the rotation angle based on linear regression and deep learning, both models had relatively large confidence intervals. The deep learning model was found to be 20% more accurate than the linear regression model.

Correcting or estimating a rotation on a single-view radiograph gives some knowledge about the differences between a rotated or non-rotated femur. However, they do not clarify which shape variations described by 2D SSMs are influenced by rotation. For this, the shape modes themselves need to be studied further.

In this thesis, two experiments will be described. In the first experiment, inspired by Väänänen et al. [14], the effects of projection will be investigated by analysing how 3D landmarks of the proximal femur are affected during projection. Different 3D shape modes will be projected at neutral angle (0°). Furthermore, the mode describing the most shape variance will be projected at different angles (-30° , 0° and 30°).

A second experiment aims to quantitatively clarify the contribution of femur rotations to the shape variations described by a 2D femoral SSM. The approach involves generating 2D radiographs from CT scans at various angles, allowing for a reverse-engineering process to include the rotation angle in 2D SSM shape parameter data. By examining how different angles influence the SSM's modes, using boxplots and an analysis of variance, this study seeks to isolate the effects of rotation from actual shape.

2

Methods

To investigate the impact of femoral rotation on the representation of femoral shape in X-rays, it is necessary to describe the methods by which femoral shapes within a population. This involves understanding the principles of a Statistical Shape Model (SSM) and the process of constructing these models. The first experiment aimed to generate a 3D whole femur SSM based on segmented CT studies sourced from the APPROACH dataset and analysed the proximal femur 2D projections. The second experiment involved the creation of digitally reconstructed radiographs (DRRs) from CT studies also from the APPROACH dataset. These DRRs are created by rotating the CTs and simulating an X-ray projection, simulating internal and external rotation. The resulting DRRs were then used to create two different 2D SSMs. One 2D SSM was created by expanding an existing SSM's data based on the WorldCOACH dataset and adding the DRRs to the available data. For this, the landmark protocol of the DRRs was aligned with WorldCOACH's. A second 2D SSM was created by using only data from the DRRs. For this thesis, different SSMs were made using different methodologies. Most shape models were made from scratch according to the method described below, whereas the different models involving data from WorldCOACH are made with BoneFinder [15].

2.1 Basics of Statistical Shape Modelling (SSM)

In the study of bones, understanding the variability in shape or density among different individuals is important in various applications. Statistical Shape Models (SSM) have emerged as a powerful method to systematically capture, analyse, and interpret these variations in shape. The fundamental principle of SSM is the mathematical representation of the shape of objects (in this context, bones) in a way that quantifies the variations across a population. To construct a SSM, the process begins with acquiring a shape representation. In the context of bone shapes, landmarks are most frequently used [8]. Each landmark is defined by its coordinates, which can be written in vector form to facilitate mathematical operations and analysis. In a 2D model based on n landmarks, the i^{th} bone sample in the dataset will be represented as:

$$\mathbf{x}_i = [x_1, y_1, x_2, y_2, \dots, x_n, y_n]^T \quad (2.1)$$

In a 3D model, the vector extends to include the z coordinates:

$$\mathbf{x}_i = [x_1, y_1, z_1, x_2, y_2, z_2, \dots, x_n, y_n, z_n]^T \quad (2.2)$$

Once the landmarks have been placed on the imaging data, such as CT scans or radiographs, and their correspondence established, it is essential to align these landmarks. This alignment is necessary for reducing sample variability due to non-shape factors. It involves Procrustes analysis, which corrects for translation, rotation, and isotropic scaling. Doing so eliminates pose-related variations, ensuring that subsequent analyses reflect actual morphological differences. The next step is to apply Principal Component Analysis (PCA), which identifies the principal modes of variation within the bone samples [16].

The first step of PCA is to calculate the average shape, $\bar{\mathbf{x}}$, of the population. This can easily be calculated as

$$\bar{x} = \frac{1}{N} \sum_{i=1}^N x_i \quad (2.3)$$

where N is the number of samples. Using the average shape and comparing this to the variation of different shapes x_i , the covariance matrix, S , can be calculated. This is described as:

$$S = \frac{1}{N-1} \sum_{i=1}^N (x_i - \bar{x})(x_i - \bar{x})^T \quad (2.4)$$

The eigenvectors of the covariance matrix S , ordered by their corresponding eigenvalues in descending order, represent the principal modes of variation. The eigenvalues indicate the amount of variance captured by each mode. In the context of an SSM, each eigenvector or principal mode (ϕ) represents a specific pattern of shape within the dataset. These modes are orthogonal to each other, ensuring that each captures a unique aspect of shape. Each eigenvalue (λ) reflects the importance, or weight, of its corresponding eigenvector in capturing the shape variability in the dataset. Larger eigenvalues correspond to modes of variation that explain a more significant proportion of the total variability.

A shape x_i from the population can be approximately reconstructed using a linear combination of the mean shape and the principal modes weighted by their corresponding scores:

$$x_i \approx \bar{x} + \sum_{m=1}^M b_{m,i} \phi_m \quad (2.5)$$

Where

- \bar{x} is the mean shape vector.
- $b_{m,i}$ are the weights or scores for the i^{th} shape on the m^{th} mode.
- ϕ_m are the eigenvectors representing the principal modes of variation.
- M is the number of modes retained for the model, typically selected based on the cumulative variance they explain.

Often, models are limited to a maximum of 3 standard deviations. This is done by limiting the weights of the model to:

$$-3\sqrt{\lambda_m} \leq b_m \leq 3\sqrt{\lambda_m} \quad (2.6)$$

where b_m and λ_m are the weight and the eigenvalue of the m^{th} mode respectively.

2.2 Datasets

This thesis utilised two primary datasets: the APPROACH dataset, which includes full-body CT scans, and the WorldCOACH dataset, consisting of hip X-rays.

APPROACH Dataset: The primary dataset for this thesis is the APPROACH dataset, which contains 250 full-body CT scans. However, only 99 of these scans were selected for analysis in this study; the rationale is explained later in Section 2.3.1. These scans include 99 patients (58 females, with an average age of 66.8 ± 6.2 years; 20 males, with an average age of 68.1 ± 5.6 years; and 21 with unknown sex and age). The scans were performed in the transverse plane using various acquisition parameters and CT modalities from several manufacturers, including Philips, Toshiba, GE, and Siemens.

WorldCOACH Dataset: The WorldCOACH dataset includes 67,448 X-ray scans of hips gathered from previous research studies. These scans were performed with differing acquisition parameters. A detailed overview of the different cohort studies in the WorldCOACH dataset can be found in Table 2.1.

Table 2.1: Table with all the cohorts of WorldCOACH including size

Cohort	Size
APO	1,392
Chingford	1,760
JoCo	7,392
MOST	6,015
OAI	9,413
RS1	11,686
RS2	4,606
RS3	6,001
SF	16,577
TASOAC	2,264
WorldCOACH (total)	67,448

2.3 Experiment 1: 3D SSM of the femur and its 2D projection

The objectives of the first experiment were to see what shape variation exists in a 3D femoral SSM and to investigate the effects of their projection in 2D. This involved a comparative analysis between a 3D SSM of the femur and its 2D projection.

The 3D SSM was built following methods similar to those described by Nora Baka et al. [17], using CT scans of the APPROACH dataset. Correspondence among these scans from different patients was established by segmenting the femurs and registering them. For this, Elastix [18] was used. The landmarks were created by taking a uniform point sample from one of the 3D surfaces resulting from segmentation. The registration transformations were applied to the landmarks to prepare the data for Principal Component Analysis (PCA).

2.3.1 From full-body CT to segmented femur

As the focus of this thesis is on the femur, the region of interest was narrowed down from the available full-body scans. This was done by removing extraneous slices from the full-body scans. The segmentation was performed using Riccardo Biondi's graph-cut-based algorithm with default parameters [19]. The CT was first split along the sagittal plane, then normalised, followed by the graph-cut segmentation. Lastly, the segmentation got morphologically closed using a flood-fill algorithm, and the largest component was kept. The result is a binary image that can be saved in the same format as the CT scans. The nearly raw raster data (.nrrd) file format was used for this thesis. Other formats like nifti (.nii) can also be used as long as these formats are compatible with other applications used in post-processing.

During the saving of these segmentations, some files were corrupted. These scans were excluded from the study. The rest were manually checked and corrected in 3D Slicer [20]. Common errors like incomplete segmentation or accidental inclusion of the acetabulum were addressed. As seen in Figure 2.1.

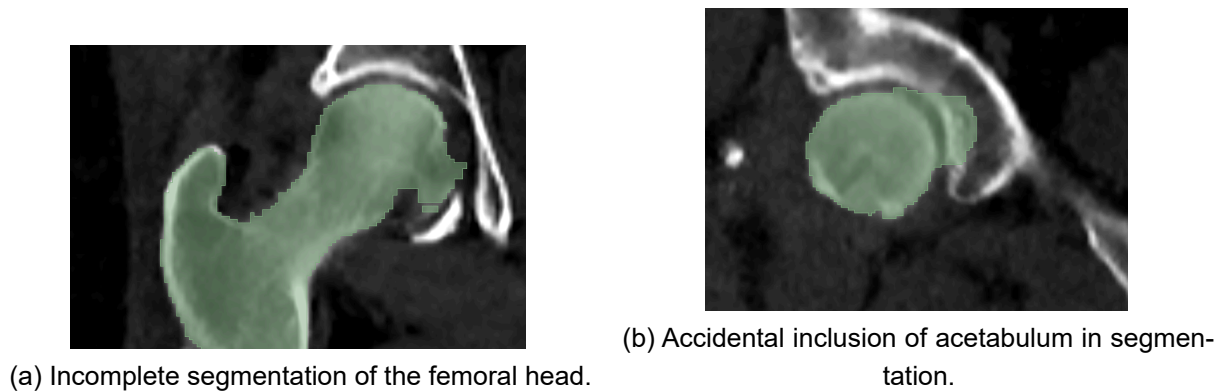


Figure 2.1: Common errors made by the segmentation algorithm, during quality control.

2.3.2 Creating landmarks and correspondence in 3D

The process begins by selecting a set of landmarks on one image, known as the fixed image, to which all other images are registered. The outcome of these registrations is a set of transformations that can be inversely applied to the landmarks, establishing correspondence across different 3D images.

Registration for Statistical Shape Model

The first step of registration is choosing a fixed image. The fixed image is selected based on the clarity of its segmentation and the resolution of the CT scan. For this thesis, the right femur of a patient with a high-resolution CT and clear segmentation was chosen as the fixed image.

Registration involves aligning two or more images of the same scene to facilitate precise comparison, integration, or analysis. In this case, the rest of the CT images were aligned (moved, in registration terms) to a fixed CT image. To improve the registration speed, one can use the binary segmentations of the images to construct the 3D statistical shape model. The Euclidean distance transform, as detailed by Maurer et al. [21], was applied to enhance this process. This transform significantly reduces computational demands and enhances the quality of registration [22], [23]. The `SignedMaurerDistanceMapImageFilter` from the Insight Toolkit (ITK) was specifically used for this purpose and applies only to binary images such as masks or segmentations.

Following the application of the distance transform, the segmentations undergo registration with Elastix [24],[18], using parameters consistent with those used by Baka et al. [17]. While most default settings were maintained, some adjustments were made to allow iterative refinement across multiple resolutions. The registration process consisted of three sequential stages:

- **Rigid Registration:** Establishes the basic alignment of the images.
- **Affine Registration:** Builds on the rigid registration to adjust scaling and fine-tune the alignment.
- **B-Spline Registration:** Uses the affine registration as a baseline to apply local transformations for detailed fit.

An important setting in this process was the `FinalBsplineInterpolationOrder`. This was set to zero for binary images and 3 for distance transforms like the Maurer Distance Transform. After registration, the resulting transforms were used to establish the correspondence of landmarks.

Establishment of Correspondence

After the registration process, the resulting transformations were applied to landmarks. This step is crucial for establishing a correspondence of points across the examined bone set. The procedure for generating landmarks began by importing the binary segmentation image of the fixed femur into 3DSlicer. Using 3DSlicer's export function, a Stereolithography (.stl) file was created, containing a detailed tri-

angle mesh with 749,722 points and 249,988 triangles [20]. From this mesh, 5,000 random points were uniformly sampled using the uniform sampling function of Open3D implementation in Python [25]. However, some points were thrown away if they were unnecessary to keep the 95th percentile of the curvature (calculated with the surface normals of the landmarks), leaving 4922 points.

It is important to note that various point-sampling methodologies might be more appropriate depending on the specific requirements of the study. For example, as demonstrated by Campoli et al., Gaussian sampling provides a probability-based approach that could offer a better representation of complex anatomical features using fewer points [26]. Alternatively, employing a gradient descent energy function, as discussed by Gaffney et al., could optimise point distribution based on minimising energy within the system [6]. Additionally, for anatomical structures like the trochanters, which demand a higher point density for accurate depiction, Fourier Analysis can be applied to determine the optimal sampling rate using the Nyquist Frequency, a technique explored in the work of Mineo et al. with point clouds [27].

This process of point sampling yields landmarks for the fixed femur, including the coordinates of these points. However, to establish a correspondence of points across all bones in the study, it is necessary to apply the transformations derived from the registration phase inversely.

Performing PCA for SSM

Once corresponding points have been established across the examined bone set, pose variations are mitigated through Procrustes analysis. This step involves adjustments for translation, rotation, and isotropic scaling. By using the SciPy Spatial Procrustes function, the methodologies developed by Gower and Krzanowski are utilised [28].

Following this, Principal Component Analysis (PCA) was applied to the coordinates to identify and quantify the model's principal shape modes. The PCA process began with the computation of the covariance matrix from the data. Eigenvalues and eigenvectors were then extracted from this matrix.

Although Kernel PCA could offer a nuanced approach by addressing non-linearities, its adoption in 3D SSMs remains minimal. A possible explanation for this is the lack of robustness of non-linear methods in 3D statistical shape modelling, as noted by Heimann et al. [29]

To interpret the shape variations captured by each mode, calculations are performed to generate shapes at both extremes of the spectrum ($\pm 3SD$), described in Equation (2.6) represented mathematically as:

$$x_m = \bar{x} \mp 3\sqrt{\lambda_m}\phi_m \quad (2.7)$$

3D Model Projected

From the set of 4,922 points in the 3D SSM, 48 key landmarks were selected, comparable to those specified in Appendix A. These landmarks, critical for analysis in Experiment 2 (Section 2.4), were chosen to study behaviour during projection onto a 2D plane. As the key landmarks are only in the proximal part of the femur, the projections were only performed on the proximal part of the femur. Multiple projection plots were generated to observe how these landmarks behave within the 3D SSM. The initial analysis observes the movements in the first three SSM modes. Additionally, the first mode, which accounts for the most variance, was examined under internal and external rotations at -30 and 30 degrees, accomplished by applying Equation (2.8) to the landmarks.

For a standard projection in the coronal plane (y -direction), only the x, z -coordinates of the landmarks are plotted. The internal and external rotation is described by a rotation around the axis in the superior direction, in this case the z -axis. To rotate the bone around this z -axis, new coordinates are calculated using Equation (2.8). After which y' -coordinate is excluded from the plot.

The following equation mathematically represents the rotation:

$$\begin{pmatrix} x' \\ y' \\ z' \end{pmatrix} = \begin{pmatrix} \cos(\theta) & -\sin(\theta) & 0 \\ \sin(\theta) & \cos(\theta) & 0 \\ 0 & 0 & 1 \end{pmatrix} \begin{pmatrix} x \\ y \\ z \end{pmatrix} \quad (2.8)$$

Here x, y and z represent the initial three-dimensional coordinates of the landmarks. The angle θ is the anticlockwise rotation around the z -axis, and x', y', z' are the coordinates after rotation.

2.4 Experiment 2: Digitally Reconstructed Radiographs (DRRs) and 2D SSMs

While Experiment 1 focuses on the qualitative exploration of a 3D SSM and the behaviour of landmarks when projected, Experiment 2 adopts a more quantitative approach, starting with 2D projections of 3D shapes. This experiment reverses the first methodology by utilising Digitally Reconstructed Radiographs (DRRs) derived from 99 CT scans in the APPROACH dataset. Two distinct 2D Statistical Shape Models (SSMs) are constructed from these: one model uses only DRR data, while the other combines DRR with data from the WorldCOACH project. To assess the influence of rotation on each mode, the b -values from Equation (2.5) are analysed statistically through boxplots and ANOVA. This analysis quantifies the impact of rotation and allows for comparing the SSM outcomes with those from Experiment 1.

2.4.1 Creation of DRRs

DRRs are generated using the `RayCastInterpolateImageFunction` from the Insight Toolkit (ITK) [22]. The first step involved aligning all CT scans through rigid registration, ensuring uniform orientation and positioning across the dataset. Then, the ray distance was set at 1000mm according to a standard proximal femur protocol [30]. The threshold was set at 0 Hounsfield Units. The focal point is positioned to closely approximate the centre of the femoral head, guided by the 3D segmentations obtained from a preceding experiment. A total of 13 DRRs were generated for each scan, covering angles from -30 to 30 degrees in 5-degree increments, resulting in a total of 1287 DRR images. An example of a DRR produced at 0 degrees, each with a resolution of 750x750 pixels, is shown in Figure 2.2.

2.4.2 Creating contours

Along with the DRRs derived from CT scans, additional DRRs were generated from 3D segmentations under the same parameters. This involves using the `BinaryContourImageFilter` from ITK to create contours from these DRRs. The resulting contours are overlaid onto the DRRs, providing a detailed outline of the bone's three-dimensional structure from the chosen viewpoint. This contour facilitates more accurate placement of landmarks in subsequent steps.

2.4.3 Creating Landmarks on the DRRs

Landmarks are manually placed on the contoured DRRs using BoneFinder [15]. The landmarks are placed manually according to the protocol described in Appendix A. An example of such placement can be found in Figure 2.2.

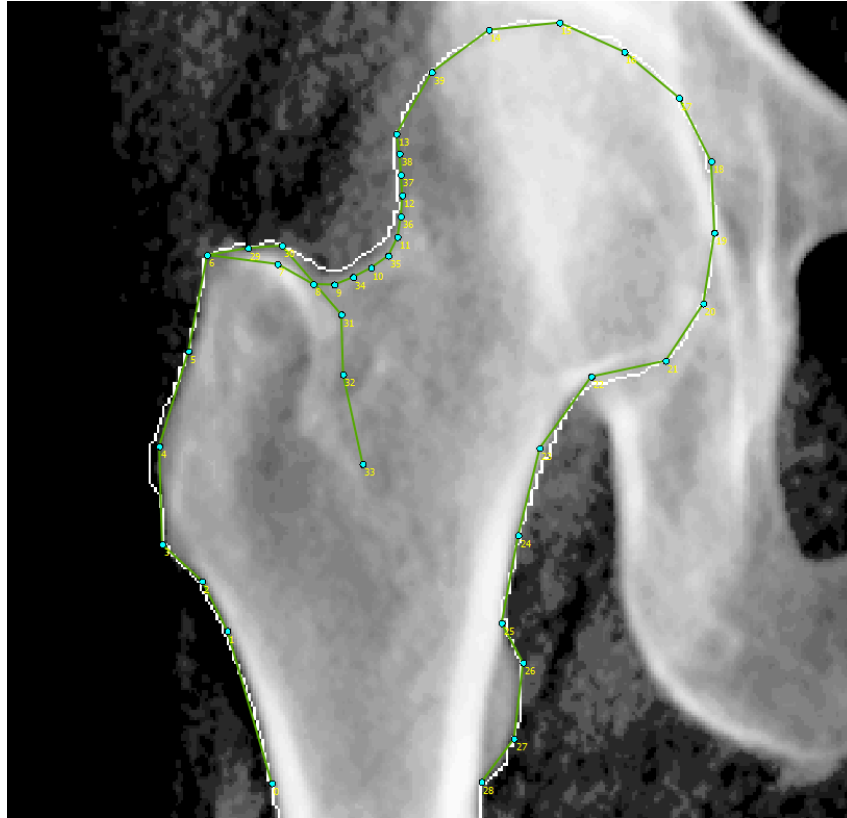


Figure 2.2: An example DRR in neutral position (0°), including contour and landmark placement according to Appendix A.

2.4.4 Creation of 2D SSMs

The landmarks from the DRRs were merged with corresponding landmarks already placed on 67,448 radiographs from the WorldCOACH dataset. This combined data was utilised to develop a 2D SSM using BoneFinder. Integrating the DRR and WorldCOACH datasets into a single 2D SSM made it possible to conduct analysis on the shape variations caused by internal and external rotations within the WorldCOACH dataset.

Also, a 2D SSM was made using only the DRR landmark data. This model was created from scratch by first applying Procrustes analysis to the landmarks. Later, PCA was applied to these points to create a 2D SSM.

2.4.5 Analysis of the resulting b -values

Each CT scan from the APPROACH dataset produced a series of DRRs across various angles, which could be analysed using the statistical model defined in Equation (2.5). This model included a set of b_m values for each mode, representing the shape variations.

To visualise these variations, the mean bone shape vector \bar{x} was combined with the mode-specific eigenvector (ϕ_m) multiplied by a mode-specific weight (b_m). The weights were adjusted between $-3SD$ and $+3SD$ for each plot. Furthermore, the b_m -values for each DRR angle are compared with those from WorldCOACH, with data segmented into different cohorts as specified in Table 2.1.

To ensure a robust comparison between the DRRs and WorldCOACH data, all values were normalised by subtracting the mean and dividing by the standard deviation. This normalisation centres the mean at zero and expresses the b values in terms of standard deviations:

$$\frac{b_m - \mu_m}{\sigma_m} \quad (2.9)$$

Where b_m is the value of the parameter corresponding to the mode in Equation (2.5) and μ_m and σ_m are the mean and standard deviation of the parameters of the corresponding mode.

A series of boxplots was generated to provide a statistical summary of the b values for each mode, arranged side by side for each angle. The mean values extracted from the boxplots were used to construct a trend curve, representing the mean b value as a function of the rotation angle. This curve, along with individual cases, visually validated the representativeness of the mean trend curve.

The b values in an SSM capture the shape configuration of a bone. In 2D representations, these values can be influenced by either rotation (leading to perceived or artificial shape changes) or the inherent characteristics of the individual bone (reflecting true shape variations). To ensure statistical validity, Levene's test was first conducted to assess the equality of variances. Following this, a one-way Welch's ANOVA was performed for greater statistical robustness, as suggested by Liu (2015). The apparent shape for each specific mode (b_m -value) was evaluated based on two independent variables:

Bone Shape (Femur): Reflecting natural anatomical variations among different femurs.

Angle of DRR Creation: Representing the rotational angles at which the DRRs were created.

Welch's ANOVAs were conducted on the normalized b_m -values for the first five modes across two datasets: the DRR-extended WorldCOACH SSM and the DRR-only SSM.

3

Results

The outcomes of both parts of this thesis are presented. In the first part, the 3D SSM is briefly shown. The effects of projecting 3D points on a 2D surface are also shown. In the second part, two 2D SSMs are made from DRRs. One model is only based on DRR data, the other on the combination of DRRs and the larger dataset of WorldCOACH. From both, the resulting b -values are presented and analysed using Welch's ANOVA.

3.1 Experiment 1: 3D SSM of the femur and its 2D projection

The first experiment started with the creation of a 3D whole femur SSM. The explained variance is shown, and the first three modes are presented in 3D, followed by a projection of the proximal part. Only the first mode is rotated in different directions to understand how projected landmarks behave in different rotations.

3.1.1 3D Femoral SSM

The 3D SSM needs 30 modes to explain 95% of the total shape variance. The following Figure 3.1 shows the explained variance per mode for the 3D SSM.

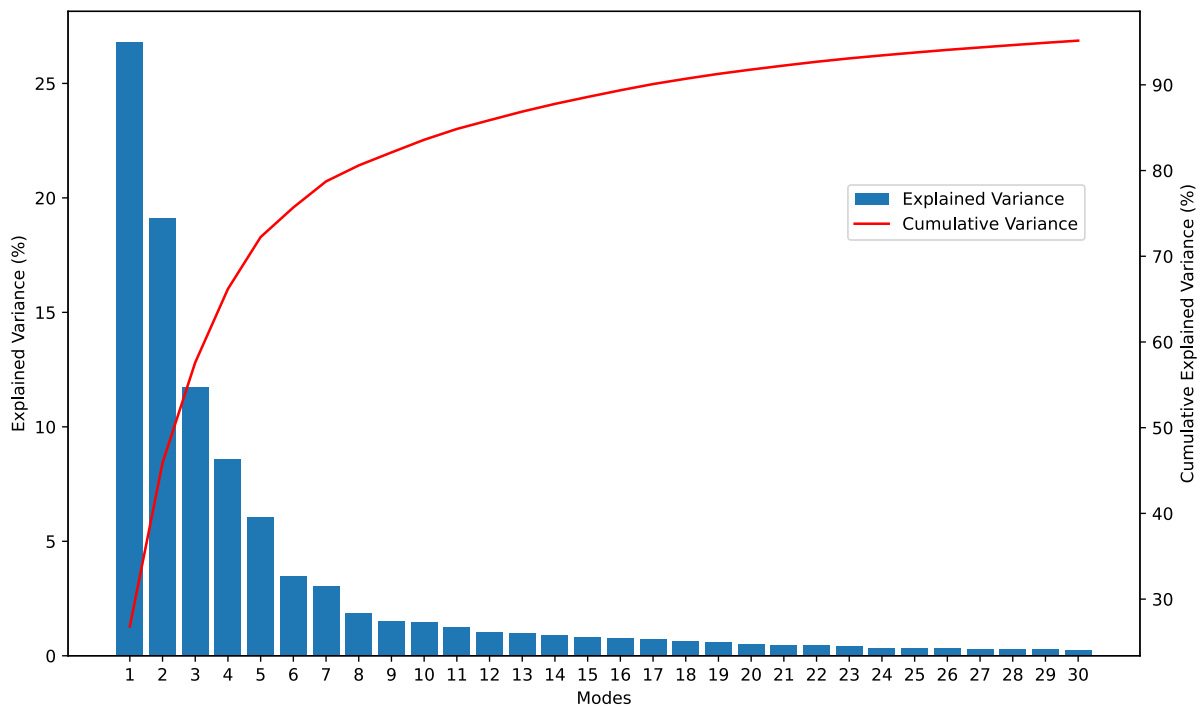


Figure 3.1: This figure shows the explained variance of each mode. To describe at least 95 % of the total variance in the whole femur, 30 modes are necessary.

Each mode in a SSM captures a specific type of shape variation among a population. What shape variations the first three modes describe are shown in Figures 3.2, 3.4 and 3.5.



(a) 3D mean shape (white) and mean-3SD (blue) shape.

(b) 3D mean shape (white) and mean+3SD (red) shape.

(c) mean-3SD shape (blue) and mean+3SD shape (red).

Figure 3.2: Shape mode 1 resulting from the whole femur 3D SSM.

Mode 1 influences the femoral neck-shaft angle. Seen in Figure 3.3. In this case, the negative standard deviation shows a decreased inclination angle (coxa vara), and a positive standard deviation shows an increased inclination angle (coxa valga).

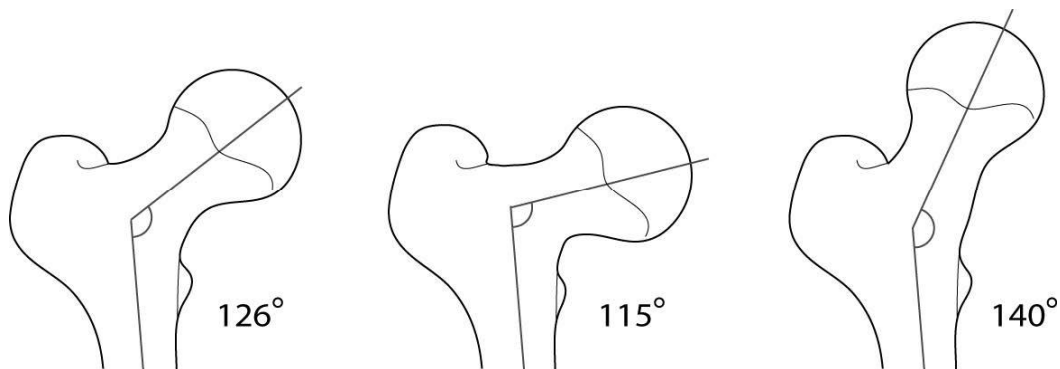
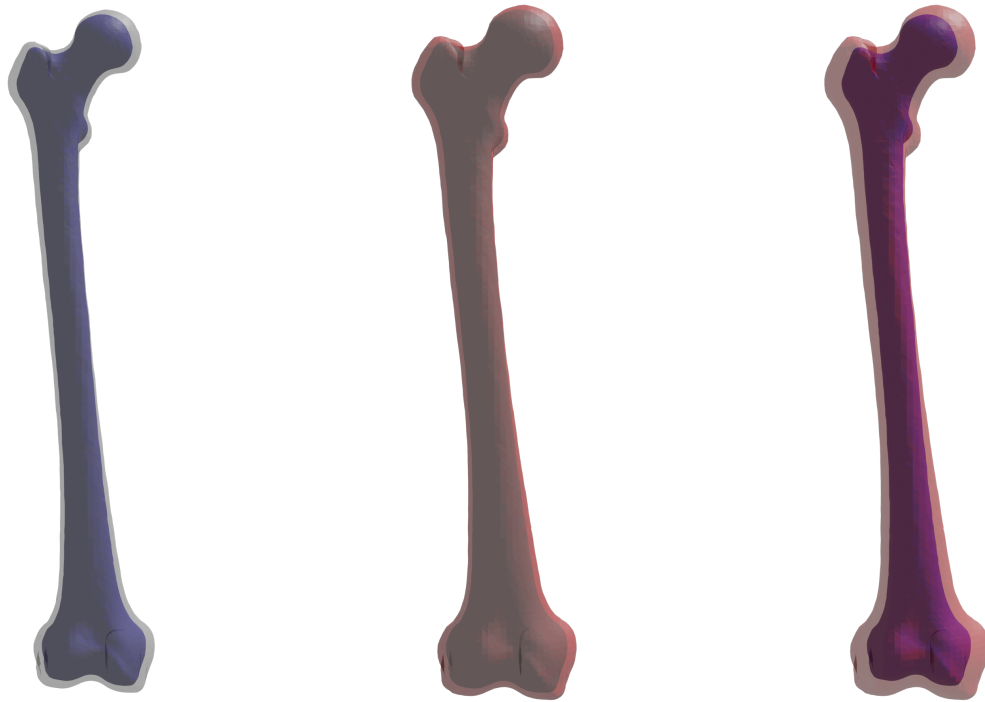


Figure 3.3: An image from Bryne et al. (a) Normal femoral neck angle, (b) a decreased femoral neck angle (coxa vara), and (c) an increased femoral neck angle (coxa valga) [31].



(a) 3D mean shape (white) and mean-3SD (blue) shape.

(b) 3D mean shape (white) and mean+3SD (red) shape.

(c) mean-3SD shape (blue) and mean+3SD shape (red).

Figure 3.4: Shape mode 2 resulting from the whole femur 3D SSM.

Mode 2 looks to influence the scale of the femur; a negative standard deviation shows a smaller femur and a positive standard deviation shows a larger femur.



(a) 3D mean shape (white) and mean-3SD (blue) shape.

(b) 3D mean shape (white) and mean+3SD (red) shape.

(c) mean-3SD shape (blue) and mean+3SD shape (red).

Figure 3.5: Shape mode 3 resulting from the whole femur 3D SSM.

Mode 3 looks to influence the anteversion (the degree of inward rotation of the femoral head relative to the knee) of the bone. Here a negative direction describes a smaller anteversion angle (retrovesion), whereas a positive direction describes a larger anteversion angle.

3.1.2 2D plots of 3D modes

The modes previously shown in 3D are now shown in 2D scatter plots; the landmarks belonging to the proximal part of the femur are plotted in blue. The previously mentioned 48 key landmarks are highlighted in red. From this perspective, all the points describe the outline shape of the bone.

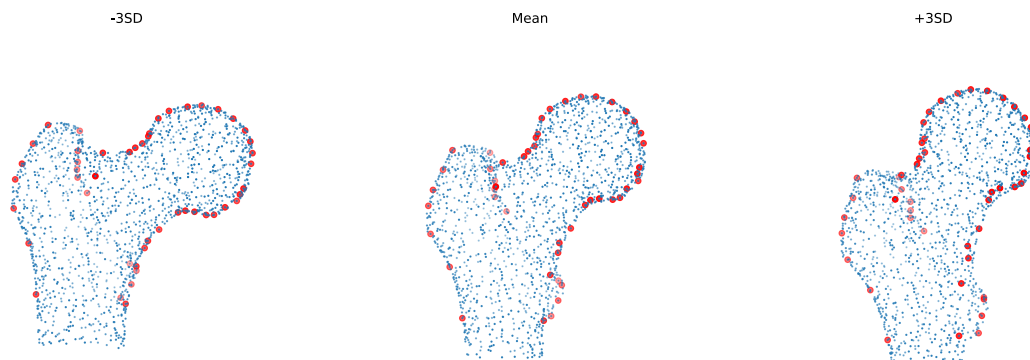


Figure 3.6: 2D projection of the landmarks (blue) described by Figure 3.2. The key landmarks are red.

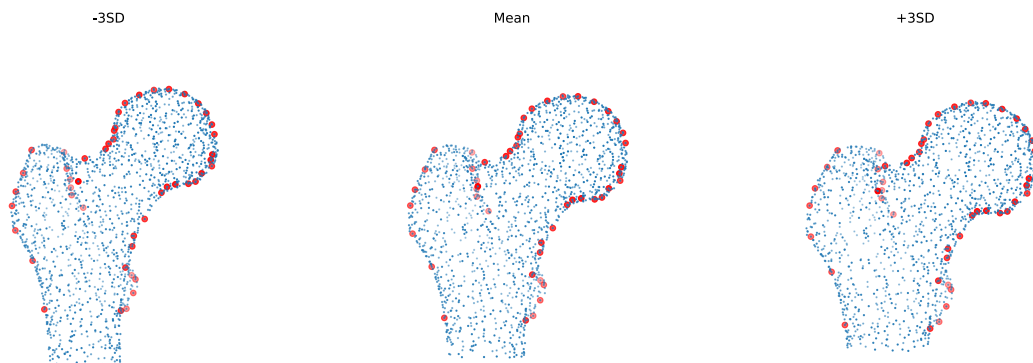


Figure 3.7: 2D projection of the landmarks (blue) described by Figure 3.4. The key landmarks are red.

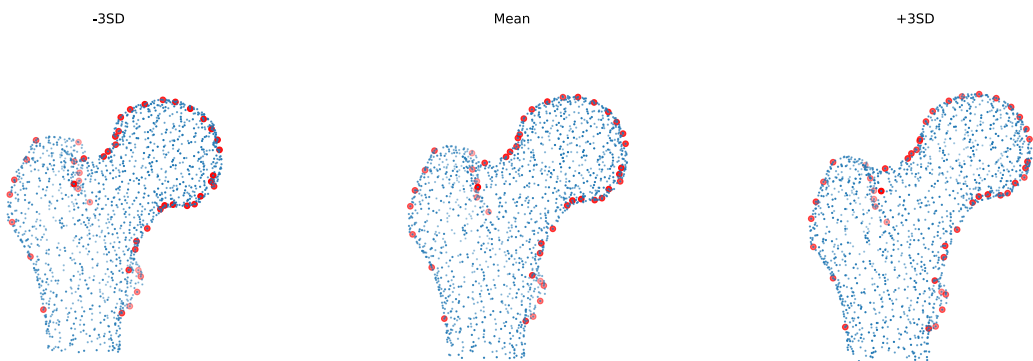


Figure 3.8: 2D projection of the landmarks (blue) described by Figure 3.5. The key landmarks are red.

The influence of rotation becomes apparent when the bones are first rotated and then projected. In Figures 3.9 and 3.10. For -30 degree rotation, especially the upper part of the greater trochanter misses some points, and a part of the femoral head is not correctly outlined, but overall, the outline looks quite accurate. The key landmarks on the 30 degrees rotation on the other hand clearly describe the outline less well, especially the head, larger trochanter and the lateral side of the femur. Although this is probably more difficult to see in 2D as the shape differences in the trochanters are on the back of our perspective. Interesting to see is the fact that the neck-shaft angle, described by Mode 1, is still well described in both directions.

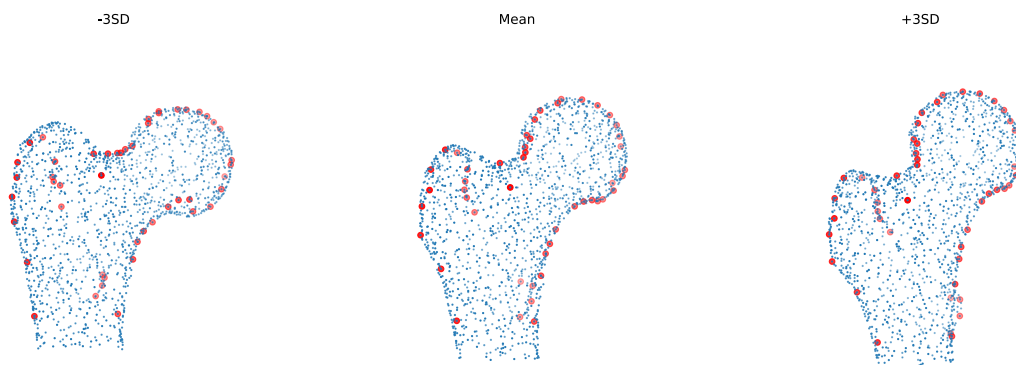


Figure 3.9: -30 degrees (internal rotation)

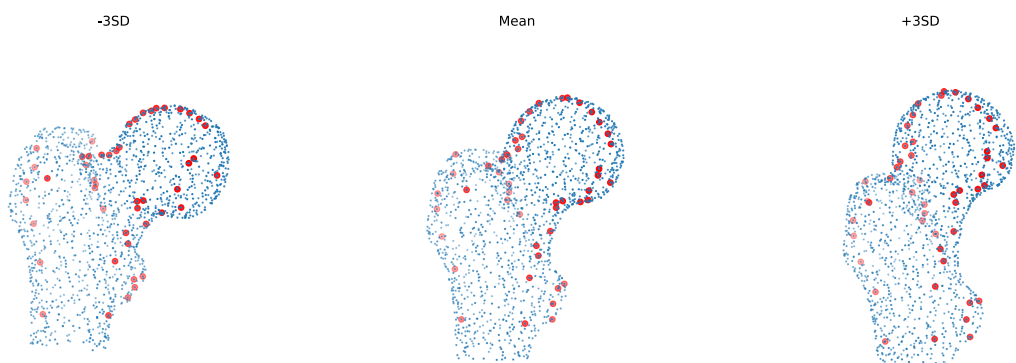


Figure 3.10: 30 degrees (external rotation)

3.2 Experiment 2: Digitally Reconstructed Radiographs (DRRs) and 2D SSMs

In the second part, two 2D SSM's were made, based on projection images. First, some examples of DRRs are presented. Then, the two SSMs are presented. The first model is an extension of the already created SSM based on the WorldCOACH dataset, of which the modes can be found in Appendix B. The model was extended with all (meaning every angle) the DRRs, ranging from -30 to 30 degrees. The second model is a SSM based on all DRRs. The resulting b values are presented and analysed using ANOVA.

3.2.1 DRRs

The DRRs combined with the contours from Section 2.4.2 look like the following:

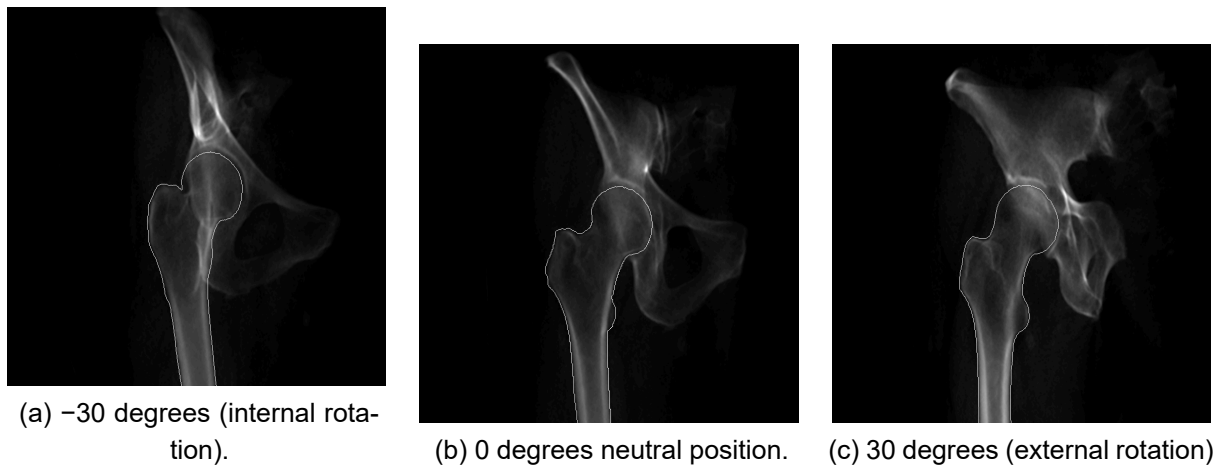


Figure 3.11: Some DRRs that were created with ITK.

Notice the lesser trochanter in Figure 3.11. At internal rotation, the lesser trochanter becomes less prominent than external rotation, as seen in Figures 3.9 and 3.10. Also, the superior junction between the femur's greater trochanter, neck and head appears differently. When the landmarks of Appendix A are applied to all DRRs and the different shapes are analysed, the following mean shapes are the result:

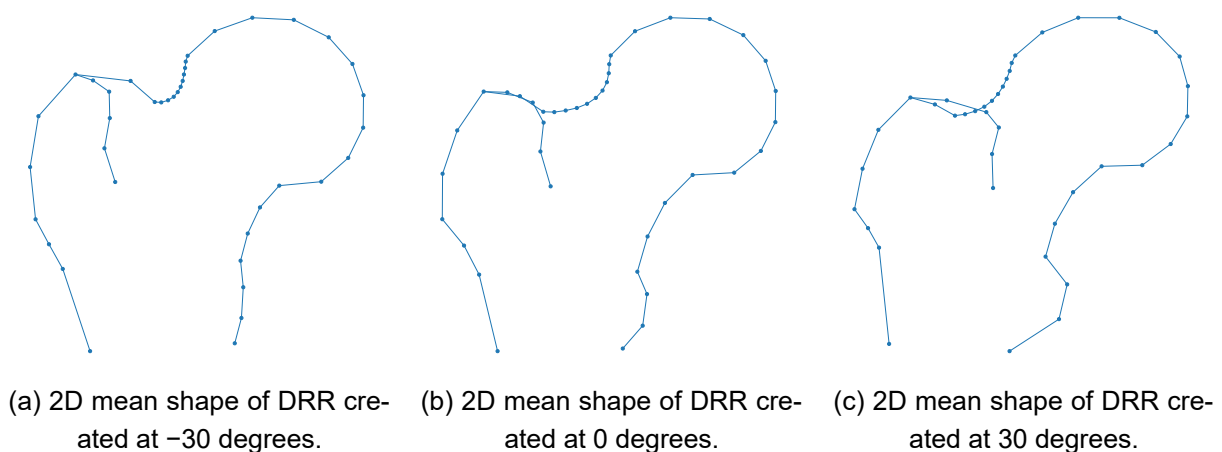


Figure 3.12: Mean shapes of DRRs at different angles.

3.2.2 2D SSMs: Shape modes

The modes of the resulting 2D models explain the variance as shown in Figure 3.14. It can be seen that the WorlCOACH model needs 19 modes to describe 95% of the shape variance, whereas the DRR model needs 16 modes. Also, mode 1 of the DRR model is dominant, describing 43.8% of the variance.

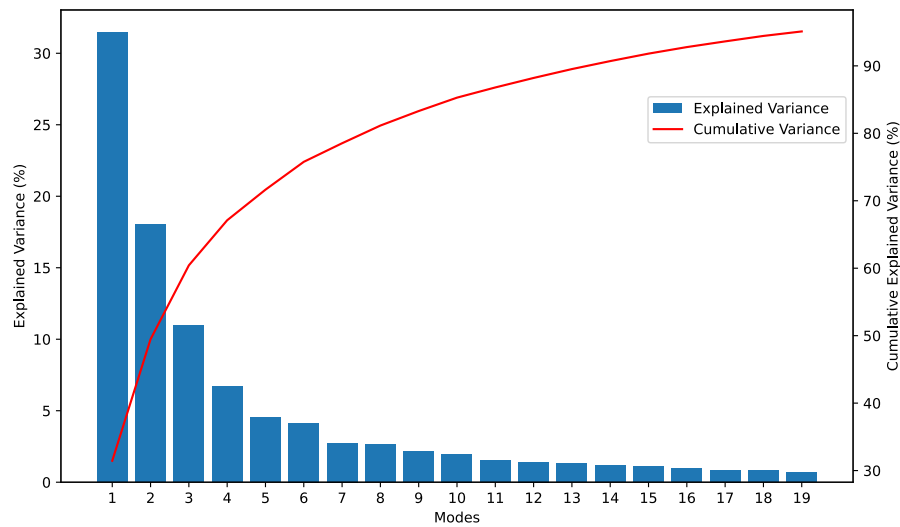


Figure 3.13: The explained variance of each mode of the WorldCOACH and DRR SSM. To describe at least 95 % of the total variance, 19 modes are necessary.

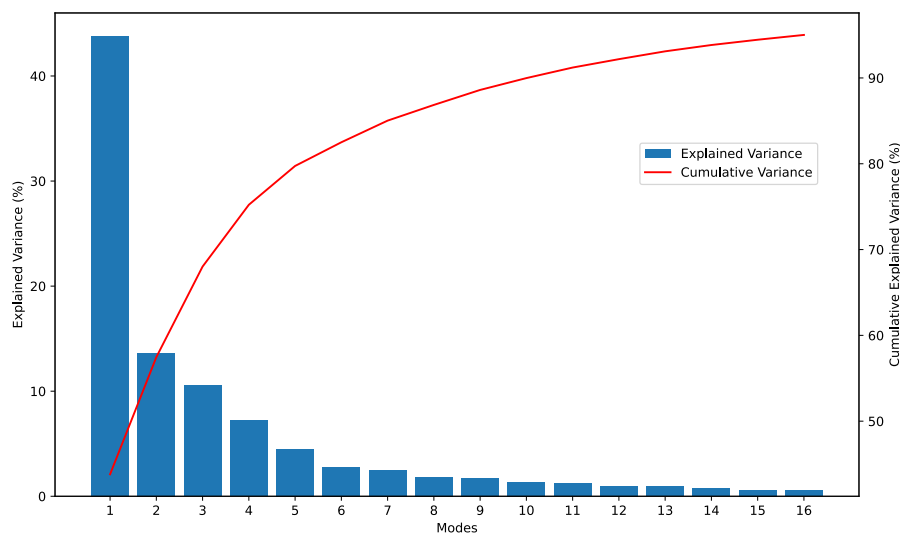


Figure 3.14: The explained variance of each mode of the DRR mixed angle model. To describe at least 95 % of the total variance, 16 modes are necessary.

Like the previous model, each mode describes a shape variation. The shape variation each mode represents is shown in Table 3.1 for the combined data SSM and Table 3.2 for the DRR-only SSM.

Combined SSM WorldCOACH and DRR

The shape variations in the combined WorldCOACH and DRR model, as shown in Table 3.1, are similar to those observed in the WorldCOACH-only model of Table B.1.

Mode 1 of WorldCOACH clearly describes the sizes of the greater and lesser trochanters combined with the neck length. A shorter neck and more prominent trochanters were associated with external rotation; see Figure 3.10 and Figure 3.12c

Mode 2 focuses on the size of the greater trochanter, combined with neck length. However, in this case, this seems independent of the lesser trochanter size. Additionally, the head at $-3SD$ becomes larger

and less round compared to the $+3SD$. In mode 2, the size difference of the greater trochanter between $-3SD$ and $+3SD$ is less compared to the size difference from $-3SD$ and $+3SD$ in mode 1. Unlike mode 1, which appears to size the greater trochanter in general, mode 2 seems to have a much more vertical size-scaling than horizontal size-scaling of the greater trochanter.

Mode 3 mainly describes the size of the greater trochanter combined with the upper neck shape. Here, it can be seen that a more negative directed value in mode 3 results in a smaller head, with a more noticeable bump at the superior junction of the femoral head and neck. When mode 3 is more positive, a smoother head-neck junction is seen. There is also a change in the shape of the greater trochanter. However, compared to mode 1 (total size) and mode 2 (more vertical scale), it clearly shows horizontal size-scaling.

Mode 4 shows a more horizontal spread greater trochanter and a more pointy lesser trochanter less smoothened over a vertical line. The trochanter major is more pointy at positive b_4 values, the neck is slightly slimmer, and the trochanter minor is larger and superior.

When Mode 5 shape differences are compared, this mode partially describes the shape of the trochanter major and the superior and inferior junction of the head and the neck. Note that almost nothing changes to the trochanter minor.

Table 3.1: First five modes of 2D SSM based on WorldCOACH and DRR's.

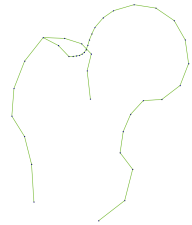
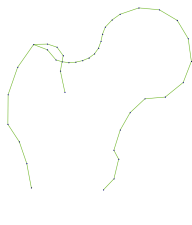
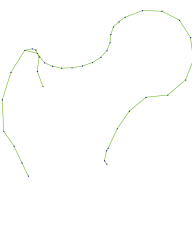
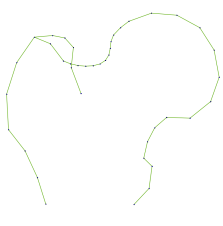
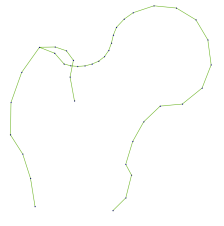
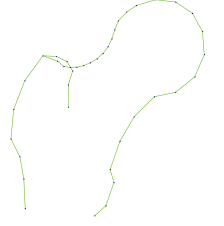
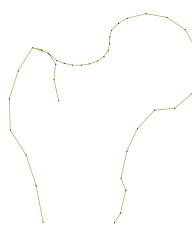
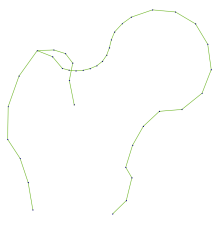
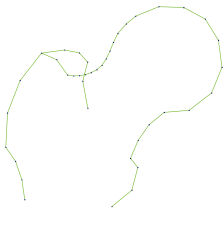
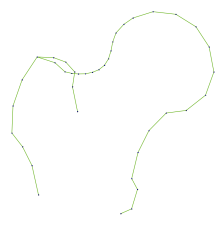
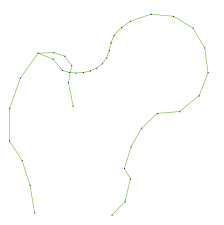
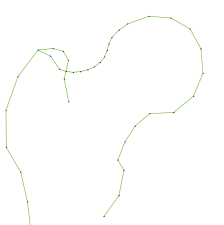
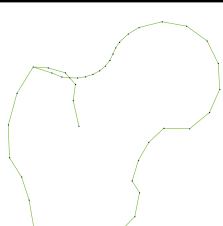
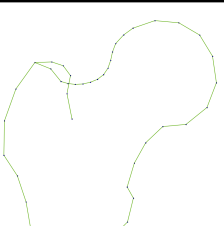
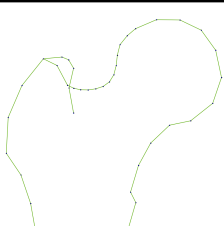
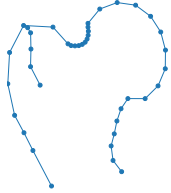
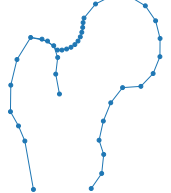
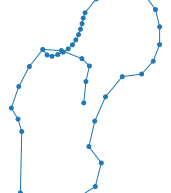
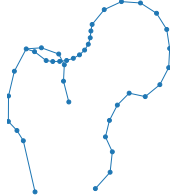
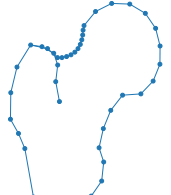
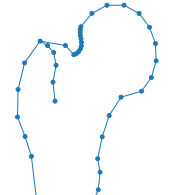
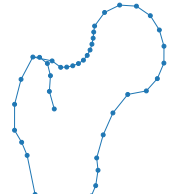
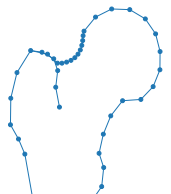
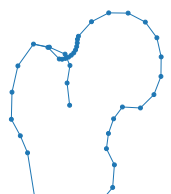
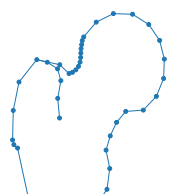
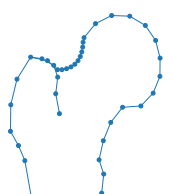
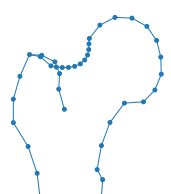
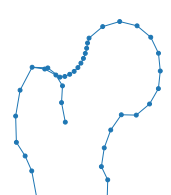
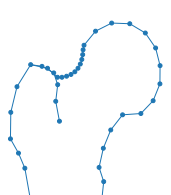
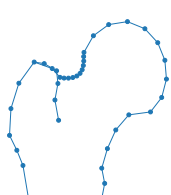
World- COACH and DRR	$b_m = -3SD$	$b_m = 0$ (Mean)	$b_m = +3SD$
Mode 1			
Mode 2			
Mode 3			
Mode 4			
Mode 5			

Table 3.2: First five modes of 2D SSM based on DRR's Only.

World- COACH and DRR	$b_m = -3SD$	$b_m = 0$ (Mean)	$b_m = +3SD$
Mode 1			
Mode 2			
Mode 3			
Mode 4			
Mode 5			

DRR Only SSM

In the DRR-only model, Mode 1 is similar to Mode 2 of the WorldCOACH model, but it also includes changes in the size of the lesser trochanter and distinct shape differences in the lateral part of the femur. A clear linear correlation is observed between the b_1 values and the rotation angle, with internal rotation leading to more negative b_1 values and external rotation resulting in more positive b_1 values.

Mode 2 in the DRR-only model describes the superior junction of the head and neck shape, along with the sizes of the greater and lesser trochanters. This mode is most affected by internal rotation, showing significant changes in shape with negative angles.

Mode 3 focuses on the size of the greater trochanter and the superior neck shape. A noticeable curve of rotational influence is present, with external rotation producing larger trochanters and internal rotation resulting in a longer neck.

Mode 4 captures variations in the lateral part of the proximal femur and the intertrochanteric line, indicating whether it is more lateral or medial. This mode shows a quadratic correlation with rotation angle, with negative shape parameters at both extremes (-30 and 30 degrees) and a top at zero degrees, see Figure 3.15 (i).

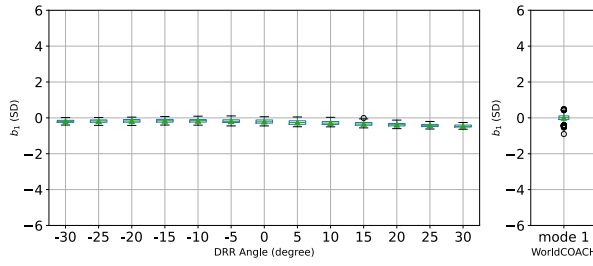
Mode 5 primarily describes the head and superior neck shapes, with a steady line of mean b_5 values across rotation angles. This indicates that Mode 5 is less influenced by rotation and more driven by population shape differences.

3.2.3 b -values: Boxplots

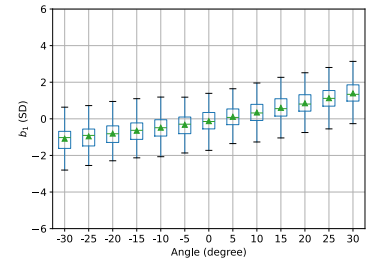
To understand the influence of rotation on b -values, boxplots were created for each angle group. The boxplots in Figure 3.15 (a)-(e) represent the combined WorldCOACH and DRR model. The boxplot of the combined model consists of two parts: the angle-grouped DRRs and the WorldCOACH data. Figure 3.15 (f)-(j) represent the DRR-only model.

In the combined model, Mode 1 shows that external rotation leads to more negative b_1 values, with the median value for WorldCOACH around 0. There is some overlap between the boxplots, making it difficult to distinguish between natural shape variation and rotation-induced variation. Mode 2 shows that internal rotation results in a shape closer to the mean b_2 value, while external rotation leads to more positive b_2 values. Mode 3 indicates that external rotation produces larger trochanters, with the DRR values shifting towards smaller b_3 values than WorldCOACH. Mode 4 shows a decreasing mean b_4 value with increasing angle, with external rotation associated with a more horizontally spread greater trochanter and a pointier lesser trochanter. Mode 5 does not show a clear dependence on rotation, suggesting that the shape changes are more likely due to natural variation.

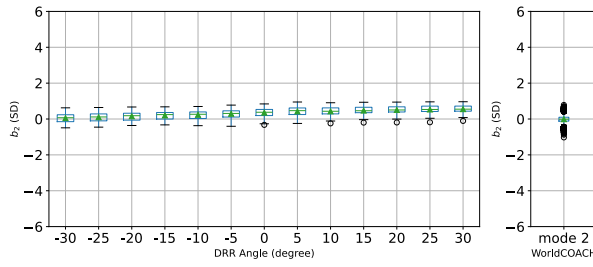
In the DRR-only model, Mode 1 exhibits a direct linear correlation between b_1 values and rotation angle. Internal rotation produces more negative b_1 values, while external rotation produces more positive b_1 values. Mode 2 shows that internal rotation has a significant impact, while Mode 3 presents a clear curve of rotational influence with external rotation, resulting in larger trochanters. Mode 4 shows a quadratic correlation with rotation angle, and Mode 5 maintains a steady line of mean b_5 values, indicating minimal influence from rotation.



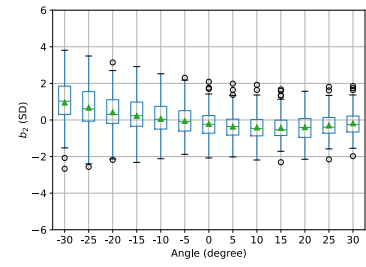
(a) Mode 1, WorldCOACH and DRR.



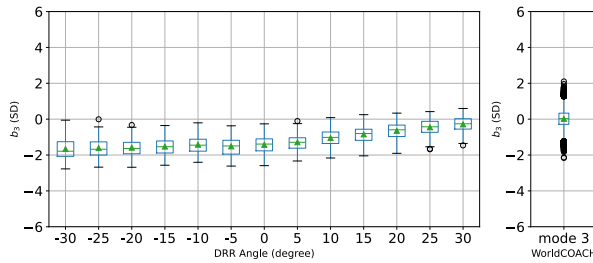
(f) Mode 1, DRR only.



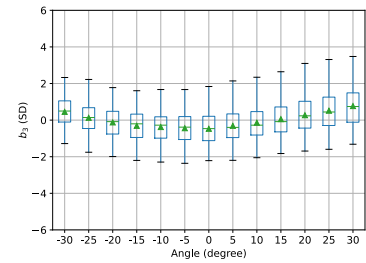
(b) Mode 2, WorldCOACH and DRR.



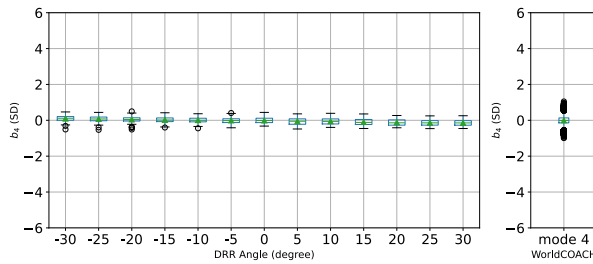
(g) Mode 2, DRR only.



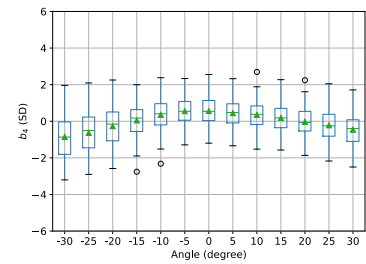
(c) Mode 3, WorldCOACH and DRR.



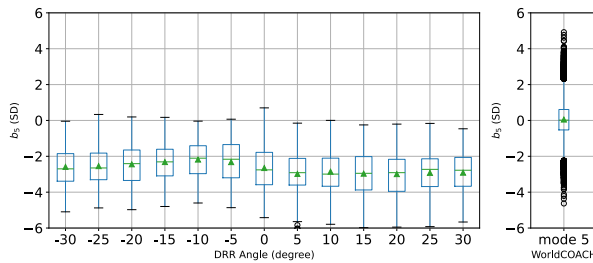
(h) Mode 3, DRR only.



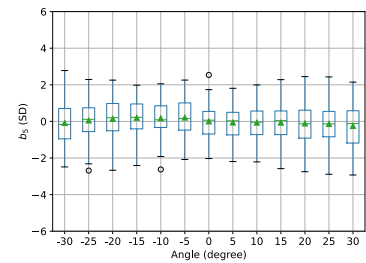
(d) Mode 4, WorldCOACH and DRR.



(i) Mode 4, DRR only.



(e) Mode 5, WorldCOACH and DRR.



(j) Mode 5, DRR only.

Figure 3.15: The boxplots of b_m -values in modes 1 to 5 of 2D SSM based on WorldCOACH and DRR data (a-e) and a 2D SSM based on only DRRs (f-j). A zoomed in version can be found in Figure C.1

3.2.4 *b*-values: Individual Curves

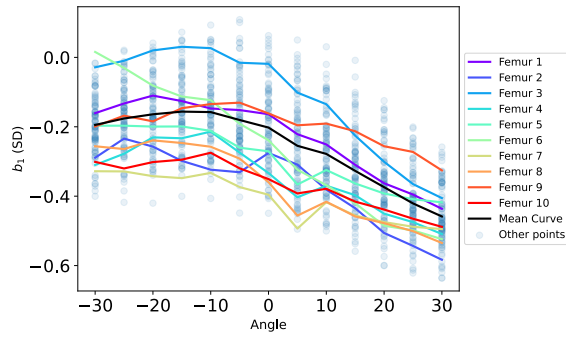
The mean values extracted from the boxplots were used to construct a trend curve, representing the mean *b* value as a function of the rotation angle. Additionally, the shape of the mean curve was plotted alongside some individual cases to validate the representativeness of the mean trend curve visually.

When observing the individual curves in Figures 3.16 and 3.17, it is apparent that most curves tend to follow the trend of the mean values. However, there are exceptions where some curves exhibit a different slope compared to the mean, and in some cases, the individual curves deviate against the trend of the mean curve. Overall, it can be said that the curves generally follow the direction of the mean curve quite well. Mode 5 is an outlier in both models, here the individual data does not consistently follow the mean curve. Some lines are straight, while others either increase or decrease, showing less uniformity.

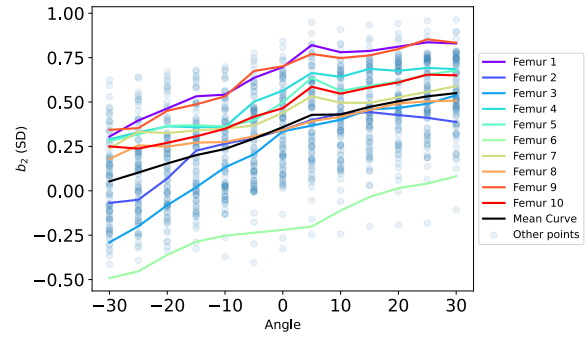
By tracking the shape-parameter values from the same bone across the angles, it becomes evident that for modes 1 to 4, the trendline of the mean curve is closely followed. This indicates a strong correlation with rotation. For example, the case of Femur 2 in mode 2 in Figure 3.17 starts at around 1 SD b_2 at -30 degrees. It ends at 2 SD at 30 degrees, illustrating how individual bones follow the general trend but with some specific deviations.

In contrast, Mode 5 shows more variability and noise, indicating less influence by the rotation angle. The individual cases in Mode 5 exhibit a wider range of behaviours, with some lines remaining straight, others decreasing, and some increasing. This suggests that individual anatomical differences are more significant in Mode 5 than other modes.

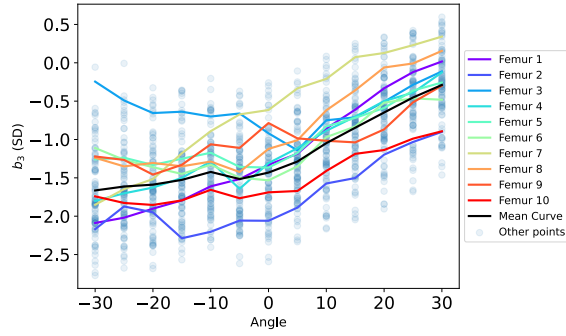
These observations make it clear that individual bone shape is crucial in determining how a mode is represented. While the mean trend provides a general overview, the individual variations highlight the importance of considering specific anatomical differences in analyses.



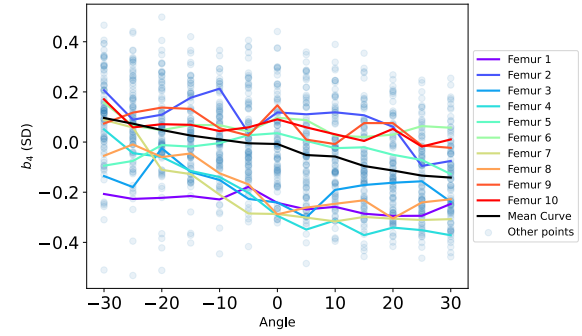
(a) Mode 1, WorldCOACH and DRR SSM



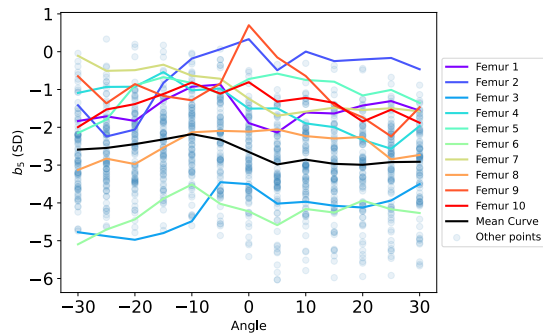
(b) Mode 2, WorldCOACH and DRR SSM



(c) Mode 3, WorldCOACH and DRR SSM



(d) Mode 4, WorldCOACH and DRR SSM



(e) Mode 5, WorldCOACH and DRR SSM

Figure 3.16: Shape variation of different modes and the b values of the rotated DRRs. The curves of the individual cases can be compared to the mean together with a scatterplot of other points.

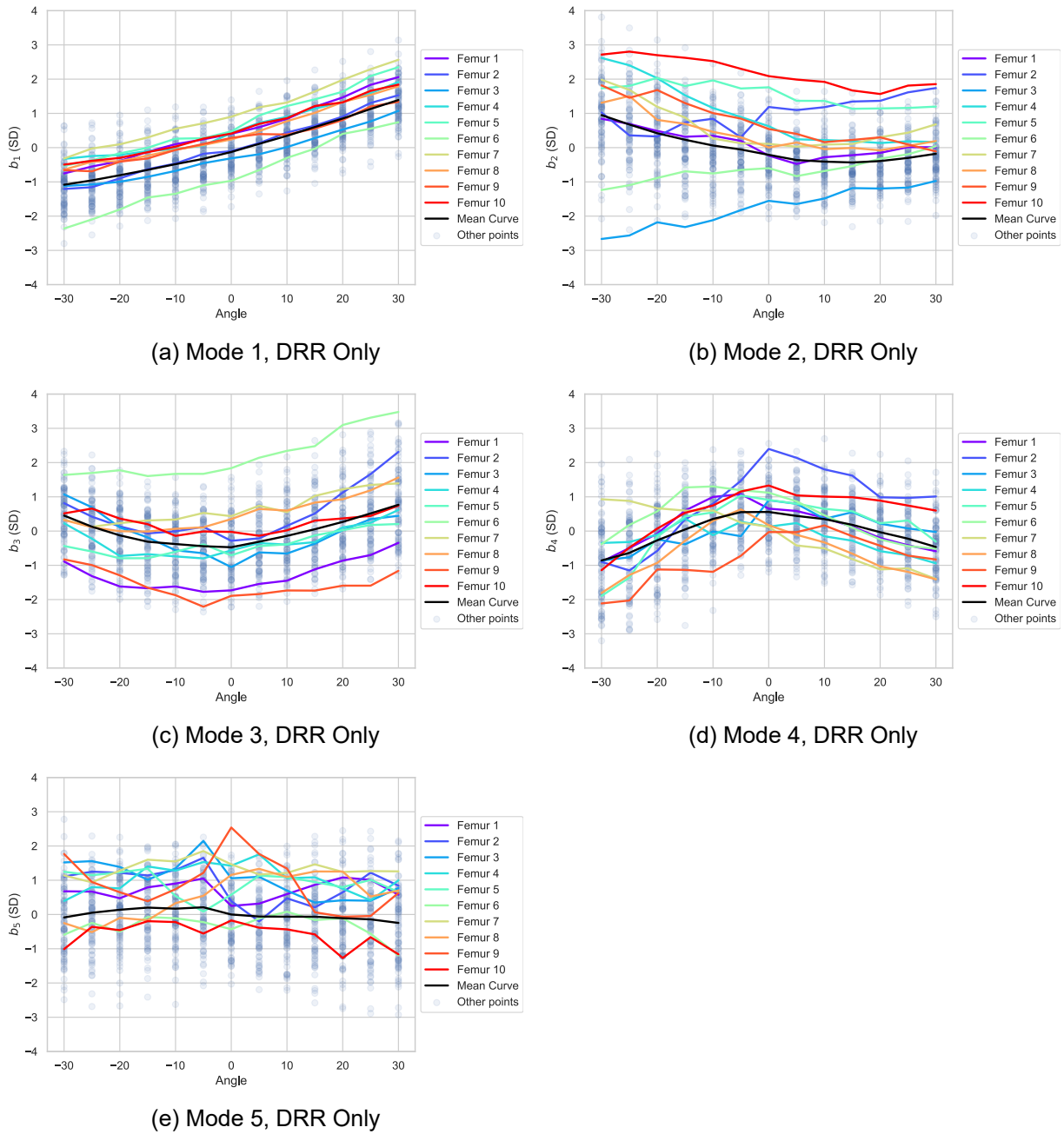


Figure 3.17: The curves of the individual cases can be compared to the mean together with a scatterplot of other points. Shape variation of different modes and the curves of individual bones within the.

3.2.5 *b*-values: Welch's ANOVA

Here are two tables presented from the Welch's ANOVA performed on the WordICOACH expanded with DRR SSM and the DRR only SSM. The variables analysed include: Degrees of Freedom 1 (DoF 1): This represents the degrees of freedom for the numerator in the F-statistic calculation. It corresponds to the number of groups minus one (98 for femurs and 12 for angles). Degrees of Freedom 2 (DoF 2): This represents the degrees of freedom for the denominator in the F-statistic calculation. It is adjusted for unequal variances and sample sizes across groups. F-statistic: A larger value indicates that the factor explains a significant amount of variability. p-value: Represents the probability of observing an F-statistic as extreme as the observed value, assuming the null hypothesis is true. The null hypotheses are that the differences in femurs do not significantly affect the PCA parameters for each mode and for the rotation Angle: The angle of DRR creation does not significantly affect the PCA parameters for each mode. Partial Eta Squared: This is a measure of effect size that indicates the proportion of the total variance that is attributed to the effect of the independent variable (either Femur or Angle).

WorldCOACH expanded with DRR SSM

Table 3.3: This table presents the results of a two independent Welch's ANOVAs performed on the shape parameter data of DRRs within the combined SSM of DRRs and WorldCOACH.

Mode	Variable	DoF 1	DoF 2	F-Statistic	p-value	Partial Eta Squared (η_p^2)
Mode 1	C(Femur)	98	404.053	11.177	<0.001	0.427
	C(Angle)	12	495.247	115.769	<0.001	0.471
Mode 2	C(Femur)	98	404.042	34.224	<0.001	0.621
	C(Angle)	12	495.357	52.278	<0.001	0.327
Mode 3	C(Femur)	98	404.047	12.679	<0.001	0.392
	C(Angle)	12	495.411	87.327	<0.001	0.442
Mode 4	C(Femur)	98	404.021	56.051	<0.001	0.692
	C(Angle)	12	495.402	20.355	<0.001	0.159
Mode 5	C(Femur)	98	404.047	43.354	<0.001	0.744
	C(Angle)	12	495.417	5.961	<0.001	0.0535

Across all five modes, significant differences were observed for both bone shape and rotation angle:

Bone Shape: The effect sizes ranged from moderate to very large, with the highest effect in Mode 5 ($\eta_p^2 = 0.744$) and the lowest in Mode 3 ($\eta_p^2 = 0.392$).

Rotation Angle: Significant effects were also observed, with the strongest effect in Mode 1 ($\eta_p^2 = 0.471$) and the weakest in Mode 5 ($\eta_p^2 = 0.053$).

DRR SSM

Table 3.4: This table presents the results of a two independent Welch's ANOVAs performed on the shape parameter data of DRR-only model.

Mode	Variable	DoF 1	DoF 2	F-Statistic	p-value	Partial Eta Squared (η_p^2)
Mode 1	C(Femur)	98	404.068	6.89	<0.001	0.367
	C(Angle)	12	495.434	162.42	<0.001	0.611
Mode 2	C(Femur)	98	404.030	33.036	<0.001	0.630
	C(Angle)	12	495.133	19.23	<0.001	0.185
Mode 3	C(Femur)	98	404.065	38.269	<0.001	0.725
	C(Angle)	12	495.344	17.301	<0.001	0.149
Mode 4	C(Femur)	98	404.032	20.926	<0.001	0.516
	C(Angle)	12	495.260	23.636	<0.001	0.198
Mode 5	C(Femur)	98	404.056	52.380	<0.001	0.746
	C(Angle)	12	495.391	1.991	0.023	0.0190

Across all five modes, significant differences were observed for both bone shape and rotation angle: Bone Shape consistently shows strong to very large effects, with the highest effect size in Mode 5 ($\eta_p^2 = 0.746$) and the lowest in Mode 1 ($\eta_p^2 = 0.367$).

Rotation Angle also shows significant effects, particularly strong in Mode 1 ($\eta_p^2 = 0.611$), with a marginally significant effect in Mode 5 ($\eta_p^2 = 0.019$).

4

Discussion

In this thesis, both 3D and 2D SSMs were developed. The whole femur 3D model, in particular, was created to gain more insight into the expected shape variations of the femur. The model also provided a hands-on understanding of the development of SSM since the 3D model has been created from scratch using methods such as registration and PCA. In contrast, the models incorporating the WorldCOACH dataset have been created using the BoneFinder tool [15].

Thirty modes describe the full 3D SSM. This is larger compared to other studies in literature [26], [6]. Campoli et al. created a model that needed 26 shape modes to describe 99% variation based on 27 CT scans. The model of Gaffney et al. described 90% of the variation within a population of 76 females with 7 or 8 shape modes, depending on the model. The 3D model from this thesis describes 90% with 16 modes. This difference in the efficiency of the model is likely due to the reduced optimisation of point placement. The 3D model of this thesis was created using a uniform point placement for the landmarks; this is not the most efficient way to describe a complete shape of the femur; complex shapes such as the proximal part of the femur are described with the same density of points as less complex parts like the shaft. Other papers in literature used algorithms like a hierarchical splitting strategy by Harris et al. [32] or a more complex algorithm like GAMES by Ferrarini et al. [33]. Nevertheless, the model still provided insight into the expected shape variations. The first three modes are similar to those reported in the literature. However, the order of modes is different [26], [6]. The first and the second shape modes are switched. This switch indicates that the femoral neck-shaft angle is more important in distinguishing shape in the APPROACH population than the other models' populations. Due to differences in populations between the studies, more variance can be included in the data used for the shape model. Therefore, different shape modes need to explain more or less variance. A supposed reason could be that gender differences in the population influence this. In the APPROACH data set, at least 58 femurs come from females, only 20 come from males, and in 21 patients, the gender is unknown. In Campoli et al., 22 samples were from men and five from women; Gaffney et al. had a population of 76 females [26], [6]. The fact that gender ratios are different for each population supports this statement; however, in a study performed by Frysz et al., it was concluded that most differences in femur do not come from gender itself but come from natural differences like in size and body composition between male and female [34]. This concludes that the ratio of male and female participants is essential in selecting a population.

Inspired by Väänänen et al. [14], the combination of the projected plots in Figures 3.6 to 3.8 and Figures 3.9, 3.10 show that 2D shape modes can be influenced by rotation. Also, it emphasises the difficulty of isolating actual shape variations from shape variations introduced by rotation. The red highlighted key landmarks show different behaviours for one rotation direction from the other. For internal rotation, the key landmarks still represent the visible outline of the bones quite well. In contrast, the key landmarks overlap less with the visible outline for external rotation.

For the second part of the thesis, both 2D SSMs show different shape variations across the presented modes. However, mode 3 represents the same kind of shape variation for both models, regarding the trochanters. In the DRR-only model, mode 3 also describes the thickness of the femoral neck. This also explains the difference of values in the Welch's Analysis for this mode. Mode 5 has an inverse relation in

shape parameter direction for both models, representing cam morphology shape appearance but with less defined shape change on the greater trochanter on the DRR-only model. What is good to see is that the shape modes of the 2D DRR extended WorldCOACH model are almost identical to the shape modes from the 2D WorldCOACH model seen in Appendix B. This allows for direct comparison between the resulting b -values of the DRRs at different angles and the b -values corresponding to the WorldCOACH dataset, resulting in the derivation of rotational angle contribution in shape modes.

Looking at the shape variations caused by each mode in Table 3.1 and Table 3.2, it is already quite challenging to distinguish between natural shape variation and shape variation caused by rotation. Noting that a broader neck and lower neck-shaft angle might reflect the effect of rotation [10] and the greater and lesser trochanter that become more or less prominent.

By looking at the mean values in subfigures in Figure 3.15, it can be seen that some mode's b -values of the DRR extended WorldCOACH model (mode 1,3) seem only dependent on the external rotation (positive) domain, whereas other mode's b -values (mode 2, 4) seem to have a positive or negative correlation with rotation. The b -values in mode 5 seem to be less dependent on the rotational angle except for the range between 10 degrees internal rotation and 10 degrees external rotation; a slight negative slope can be seen in this range. In the paper of Eckrich et al., the width of the lesser trochanter is measured at several angles, and it shows a positive correlation comparable to that of mode 2 [1]. However, one should keep in mind that these results are not directly comparable as the paper of Eckrich et al. did absolute measurements of the lesser trochanter width (in mm), and mode 2 is measured in terms of b -factor to a shape mode vector that describes more than just the lesser trochanter width. Väänänen et al. mentioned in their paper that the relation between the mode values and rotation was relatively linear for each specific bone between -20 and 20 degrees. However, the slope and intercept of the linear relation varied between bones, confirming that knowledge about the bone's neutral shape is needed to make accurate predictions about rotation.

This statement is validated when looking at, for example, a minimum value in mode 1 of the DRR and WorldCOACH model at 30 degrees internal rotation ($-0.5SD$). This has quite some overlap with other b values at different angles. This principle of overlap holds for other modes as well. From the individual cases plot in Figures 3.16 and Figure 3.17 it can be seen that most individual lines follow the trend of the mean curve quite well, especially the linear line of mode 1 in the DRR-only model (Figure 3.17a). Although some individual cases seem to undergo more change with rotation regarding the average, others barely change with rotation, for example, in mode 5 of both models. Some cases that do not follow the average trend are visible. This indicates that rotation has, on average, an influence on how specific modes appear for a bone. However, it does not necessarily have to be the case for individual cases. How much a mode's b -value changes due to rotation depends on the individual bone shape and, therefore, on the shape difference of nature. In other words, when a person has a very small lesser trochanter, the corresponding b -values will also not change much as the lesser trochanter does not appear different at another projection angle.

A Welch's ANOVA was conducted on the two SSMs to statistically prove the influence of the angle or the difference by nature. From this, it becomes clear that the angle and the natural shape differences are important for explaining observed 2D shape variation. For both models, it holds that for the first 4 modes, it could be said that these modes are more influenced by the angle than nature. For mode 5, it could be said that the mode is more influenced by shape differences caused by nature. Waarsing et al. [10] mentioned rotational effects in modes already. In their paper they mention that mode 3 of their model might reflect the rotation effect. If the above is true, this would mean that most other modes in that paper also would reflect the effects of rotation. However, modes with higher explained variance than mode 3 (modes 1 and 2) would be more affected by rotation than higher modes that describe less variance. Unfortunately, modes 1 and 2 are not mentioned in the paper of Waarsing et al. [10], so this cannot be validated.

The observation that mode 5 in this thesis is influenced more by nature than by the rotation can be explained by the fact that higher modes tend to describe more specific shapes that explain less variation. Therefore, the rotation angle is expected to influence higher modes less. It should be kept in mind that higher modes describe less variation within the population and therefore may be less relevant.

The individual lines and the ANOVA analyses point into the direction that based on one radiograph, it is very difficult to tell at what angle this projection has been made by looking at the femur alone. For this there are two possibilities to investigate further. In 2D SSMs that include a portion of the pelvis, certain modes, such as mode 7 described by Agricola et al. [5] and mode 5 by Castaño-Betancourt et al. [35], appear to represent the internal rotation of the femur in relation to the pelvis. The current method of rotation simulation, which involves rotating and projecting the entire CT scan, is not feasible when the pelvis is included. However, rotation simulation could be achievable by segmenting the femur and the pelvis in 3D and then fully separating the voxels representing the pelvis from the voxels representing the femur. By establishing a point of rotation where only the femur rotates while the pelvis remains stable, a more accurate simulation of femoral rotation relative to the pelvis could be achieved. This method could validate if the above modes truly represent rotation.

The other method is to create an experiment comparable to this thesis and estimate the true rotation of the bone by taking two images from two different directions as input. This can then be compared to other studies using two images [12], [13].

For the WorldCOACH cohorts, the b -values are expected to align with b -values in the range of -15 to -25 degrees. This matches the standard AP hip protocol, which recommends an internal rotation of 15 to 25 degrees. So, the average value in this range should be similar to the average value for the WorldCOACH cohorts, which is around 0 degrees [36]. This is not what is observed. Of the WorldCOACH expanded with DRR's SSM, only mode 4 shows b -values comparable with the situation above. A possible explanation for the b -value difference between the DRRs at -15 to -25 degrees compared to the WorldCOACH data could be the presence of additional translational and rotational components within the DRRs. The direction in which a DRR is rotated differs from a femur's natural rotation. The simulated rotation can be compared to someone standing in a neutral position and the X-ray machine taking the X-ray from another angle. In this thesis, the centre of rotation is around the estimated spatial centre of the whole femur. However, this differs from the exact spatial centre of the head of the femur. Therefore, the DRR could have some translational components. This may result in approximations of internal and external rotation not accurately reflecting the actual bone orientation, particularly for these modes. Furthermore, there could be a difference in the neutral position of the femur in the CTs. This is due to the nature of the acquisition, where patients lie on their backs. In this position, the natural position of the leg is slightly externally rotated. Also, support for the knee may have been used for some patients. Therefore, the femur could be in a slight flexion while in acquisition. Although registration was performed to align the femur bones, there could still be contributions to movements in other planes, such as sagittal and coronal planes.

Another factor to consider is the potential inconsistency in the placement of landmarks on DRRs; although the protocol (see Appendix A) is used, these landmarks are positioned manually. During the placement of points, it could be beneficial to see where the points were placed at the previous angle. This could already help decrease inconsistencies in point placement per femur as the points of the previous angle can be used as a point of reference. The source of inconsistencies becomes apparent when the points of Figures 3.9 and 3.10 are seen. Some parts, like the lesser trochanter, are not visible anymore when the bone is rotated, leading to an educated guess of where points should be. So placing points on the DRR without a reference to how the points on the previous DRR are placed could be a cause for some abrupt change in data observed at the neutral angle (0 degrees), especially seen in Figures 3.16 and Figure 3.17. This sometimes causes the individual data points to have a sawtooth shape while a smoother line is expected. To prove that a smoother line can occur between the rotation of each angle,

a separate 2D SSM can be created, which incorporates consistent point placement at different angles. For this, a 2D SSM based on the 48 key landmarks mentioned in Section 2.3.2 was created, and the data is plotted the same way as Figure 3.17; the result is the smooth/less noisy lines of Appendix D. Eventhough this results in smooth lines, it should be mentioned that this method is not a solution for the experiments in this thesis. The method involves rotating 3D points in space, which, when projected onto 2D planes, do not consistently align with the positions specified by the protocol. As a result, the landmarks may appear at coordinates different from those designated by the protocol of Appendix A.

If this second experiment was repeated, some parts could be done differently. First, one could use the existing WorldCOACH SSM and try to fit the model onto landmarked DRRs. However, in this case, it is shown that the shape modes between the WorldCOACH and the DRR extended WorldCOACH model are almost identical, so the assumption that a SSM does not change significantly as the WorldCOACH data is far greater than the set of DRRs added to the model (67,448 vs. 1,287).

Second, although the same protocol is used for placing the landmarks, the manual placement of landmarks on DRRs can introduce inconsistencies and contribute to deviations in the data. Future studies could explore automated or semi-automated methods for landmark placement to mitigate variability and improve the accuracy of shape variation assessments. See smoothed lines from Appendix D.

Third, the simulated rotation in the DRRs may not accurately represent the actual bone orientation. Further research could focus on refining DRR simulations to more closely resemble the natural rotation of the femur and account for possible movements in other planes.

Lastly, one could argue that a margin of error of 9.84% is close to a generally accepted 10%. Therefore, a smaller margin of error is preferred. To reach a margin of error below 5% with a confidence interval of 95%, a sample size of 382 would be needed, which is more than the total number of available CTs in the APPROACH dataset. To solve the availability issue in CTs, one could create a SSAM to provide more virtual bones and test the results against real bones. See the Appendix E for a SAM created with a subset of the APPROACH dataset due to memory limitations.

Future research should focus on four key areas:

Exploring Higher Modes: Investigate higher modes to better understand their sensitivity to rotation, even though these modes may represent less relevant shape variations.

Improving Rotation Simulation: Develop a model that better simulates rotation, particularly by incorporating the pelvis. This could involve segmenting the femur and pelvis in 3D, allowing for more accurate simulation of femoral rotation relative to a stable pelvis.

Validating Methods Using Radiographs: Compare the model's performance in predicting femoral rotation using two radiographs, and validate this approach against other studies that also use dual-image methods.

Leveraging Future Computational Advances: Utilise future computing power to incorporate advanced models like SAM, creating a Statistical Shape and Appearance Model (SSAM) that includes density variations in rotational differences.

5

Conclusion

In conclusion, this thesis demonstrates that the sensitivity to angle changes varies across different modes in Statistical Shape Models (SSMs). When femoral shapes are projected at different angles, they exhibit distinct variations, with some modes being asymmetrically sensitive to rotation—meaning they are more responsive to either internal or external rotation. The degree of change in a mode's b -value due to rotation is influenced by the individual bone shape and inherent anatomical differences.

The combined findings from the plots and the Welch's ANOVA analyses of two different models (DRR-only and combined WorldCOACH and DRR) show that modes 1 to 4 are more heavily influenced by the rotation angle, while natural shape differences have a greater impact on mode 5. This suggests that higher modes, which describe more specific and less variable shapes, are less influenced by rotation and more by intrinsic anatomical variations. Additionally, the individual lines and the Welch's ANOVA analyses indicate that determining the projection angle based on a single radiograph is challenging. Therefore, to gain a more accurate understanding of an individual's femoral shape, it is advisable to capture images from at least two different directions.

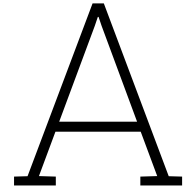
Overall, this thesis provides valuable insights into the influence of rotation on femoral shape variations, contributing to a more nuanced understanding of femoral geometry and its implications for clinical assessments and treatments.

Bibliography

- [1] S. G. Eckrich, P. C. Noble, and H. S. Tullos, "Effect of rotation on the radiographic appearance of the femoral canal," *The Journal of Arthroplasty*, vol. 9, no. 4, pp. 419–426, Aug. 1994, doi: 10.1016/0883-5403(94)90053-1°.
- [2] S. Lekamwasam, R. Sumith, and J. Lenora, "Effect of Leg Rotation on Hip Bone Mineral Density Measurements," *Journal of Clinical Densitometry*, vol. 6, no. 4, pp. 331–336, Dec. 2003, doi: 10.1385/JCD:6:4:331°.
- [3] D. C. Meyer, M. Beck, T. Ellis, R. Ganz, and M. Leunig, "Comparison of Six Radiographic Projections to Assess Femoral Head/Neck Asphericity:," *Clinical Orthopaedics and Related Research*, vol. 445, pp. 181–185, Apr. 2006, doi: 10.1097/01.blo.0000201168.72388.24°.
- [4] B. Goker, A. Sancak, S. Haznedaroglu, M. Arac, and J. A. Block, "The effects of minor hip flexion, abduction or adduction and x-ray beam angle on the radiographic joint space width of the hip," *Osteoarthritis and Cartilage*, vol. 13, no. 5, pp. 379–386, May 2005, doi: 10.1016/j.joca.2005.01.004°.
- [5] R. Agricola, M. Reijman, S. Bierma-Zeinstra, J. Verhaar, H. Weinans, and J. Waarsing, "Total hip replacement but not clinical osteoarthritis can be predicted by the shape of the hip: a prospective cohort study (CHECK)," *Osteoarthritis and Cartilage*, vol. 21, no. 4, pp. 559–564, Apr. 2013, doi: 10.1016/j.joca.2013.01.005°.
- [6] B. M. M. Gaffney, T. J. Hillen, J. J. Nepple, J. C. Clohisy, and M. D. Harris, "Statistical shape modeling of femur shape variability in female patients with hip dysplasia," *Journal of Orthopaedic Research*, vol. 37, no. 3, pp. 665–673, Mar. 2019, doi: 10.1002/jor.24214°.
- [7] M. van Buuren *et al.*, "Statistical shape modeling of the hip and the association with hip osteoarthritis: a systematic review.," *Osteoarthritis and Cartilage*, vol. 29, no. 5, pp. 607–618, 2020, doi: 10.1016/j.joca.2020.12.003°.
- [8] N. Sarkalkan, H. Weinans, and A. A. Zadpoor, "Statistical shape and appearance models of bones," *Bone*, vol. 60, pp. 129–140, Mar. 2014, doi: 10.1016/j.bone.2013.12.006°.
- [9] B. Faber *et al.*, "Subregional statistical shape modelling identifies lesser trochanter size as a possible risk factor for radiographic hip osteoarthritis, a cross-sectional analysis from the Osteoporotic Fractures in Men Study," *Osteoarthritis and Cartilage*, vol. 28, no. 8, pp. 1071–1078, Aug. 2020, doi: 10.1016/j.joca.2020.04.011°.
- [10] J. Waarsing, R. Rozendaal, J. Verhaar, S. Bierma-Zeinstra, and H. Weinans, "A statistical model of shape and density of the proximal femur in relation to radiological and clinical OA of the hip," *Osteoarthritis and Cartilage*, vol. 18, no. 6, pp. 787–794, Jun. 2010, doi: 10.1016/j.joca.2010.02.003°.
- [11] P. Lechler *et al.*, "The influence of hip rotation on femoral offset in plain radiographs," *Acta Orthopaedica*, vol. 85, no. 4, pp. 389–395, Aug. 2014, doi: 10.3109/17453674.2014.931196°.
- [12] R. Deshmukh, K. Lou, C. Neo, K. Yew, I. Rozman, and J. George, "A technique to obtain correct rotational alignment during closed locked intramedullary nailing of the femur," *Injury*, vol. 29, no. 3, pp. 207–210, Apr. 1998, doi: 10.1016/S0020-1383(97)00182-4°.

- [13] A. G. Dubina, H. S. Johal, M. R. Rozak, and R. V. O'Toole, "Can Views of the Proximal Femur Be Reliably Used to Predict Malrotation After Femoral Nail Insertion? A Cadaver Validation Study," *Journal of the American Academy of Orthopaedic Surgeons*, vol. 27, no. 24, p. e1102–e1109, Dec. 2019, doi: 10.5435/JAAOS-D-17-00505°.
- [14] S. P. Väänänen, H. Isaksson, J. H. Waarsing, A. A. Zadpoor, J. S. Jurvelin, and H. Weinans, "Estimation of 3D rotation of femur in 2D hip radiographs," *Journal of Biomechanics*, vol. 45, no. 13, pp. 2279–2283, Aug. 2012, doi: 10.1016/j.jbiomech.2012.06.007°.
- [15] C. Lindner, S. Thiagarajah, J. Wilkinson, T. Consortium, G. Wallis, and T. Cootes, "Fully Automatic Segmentation of the Proximal Femur Using Random Forest Regression Voting," *IEEE Transactions on Medical Imaging*, vol. 32, no. 8, pp. 1462–1472, Aug. 2013, doi: 10.1109/TMI.2013.2258030°.
- [16] I. Jolliffe, *Principal component analysis*. Wiley Online Library, 2005.
- [17] N. Baka *et al.*, "2D–3D shape reconstruction of the distal femur from stereo X-ray imaging using statistical shape models," *Medical Image Analysis*, vol. 15, no. 6, pp. 840–850, 2011, doi: <https://doi.org/10.1016/j.media.2011.04.001>°.
- [18] D. Shamonin, E. Bron, B. Lelieveldt, M. Smits, S. Klein, and M. Staring, "Fast parallel image registration on CPU and GPU for diagnostic classification of alzheimer's disease," *Frontiers in Neuroinformatics*, vol. 7, 2014, doi: 10.3389/fninf.2013.00050°.
- [19] R. Biondi, D. Dall'Olio, N. Curti, and G. Castellani, "A graph cut approach for femur segmentation." [Online]. Available: <https://github.com/RiccardoBiondi/FemurSegmentation>°
- [20] A. Fedorov *et al.*, "3D Slicer as an image computing platform for the Quantitative Imaging Network," *Magnetic Resonance Imaging*, vol. 30, no. 9, pp. 1323–1341, 2012, doi: <https://doi.org/10.1016/j.mri.2012.05.001>°.
- [21] C. Maurer, R. Qi, and V. Raghavan, "A linear time algorithm for computing exact Euclidean distance transforms of binary images in arbitrary dimensions," *IEEE Transactions on Pattern Analysis and Machine Intelligence*, vol. 25, no. 2, pp. 265–270, 2003, doi: 10.1109/TPAMI.2003.1177156°.
- [22] M. McCormick, X. Liu, L. Ibanez, J. Jomier, and C. Marion, "ITK: enabling reproducible research and open science," *Frontiers in Neuroinformatics*, vol. 8, 2014, doi: 10.3389/fninf.2014.00013°.
- [23] D. Rueckert and J. A. Schnabel, "Medical image registration," *Biomedical image processing*. Springer Berlin Heidelberg, Berlin, Heidelberg, pp. 131–154, 2011. doi: 10.1007/978-3-642-15816-2_5°.
- [24] S. Klein, M. Staring, K. Murphy, M. A. Viergever, and J. P. W. Pluim, "elastix: A toolbox for intensity-based medical image registration," *IEEE Transactions on Medical Imaging*, vol. 29, no. 1, pp. 196–205, 2010, doi: 10.1109/TMI.2009.2035616°.
- [25] Q.-Y. Zhou, J. Park, and V. Koltun, "Open3D: A modern library for 3D data processing," *arXiv:1801.09847*, 2018.
- [26] G. Campoli *et al.*, "Relationship between the shape and density distribution of the femur and its natural frequencies of vibration," *Journal of Biomechanics*, vol. 47, no. 13, pp. 3334–3343, Oct. 2014, doi: 10.1016/j.jbiomech.2014.08.008°.
- [27] C. Mineo, S. G. Pierce, and R. Summan, "Novel algorithms for 3D surface point cloud boundary detection and edge reconstruction," *Journal of Computational Design and Engineering*, vol. 6, no. 1, pp. 81–91, Jan. 2019, doi: 10.1016/j.jcde.2018.02.001°.
- [28] J. C. Gower, "Generalized procrustes analysis," *Psychometrika*, vol. 40, no. 1, pp. 33–51, 1975.

- [29] T. Heimann and H.-P. Meinzer, "Statistical shape models for 3D medical image segmentation: A review," *Medical Image Analysis*, vol. 13, no. 4, pp. 543–563, 2009, doi: <https://doi.org/10.1016/j.media.2009.05.004>.[◦]
- [30] A. Murphy and A. Er, "Femur (AP view)," *Radiopaedia.org*. Radiopaedia.org, May 2020. doi: [10.53347/rID-77780](https://doi.org/10.53347/rID-77780).[◦]
- [31] D. P. Byrne, K. J. Mulhall, and J. F. Baker, "Anatomy & Biomechanics of the Hip," *The Open Sports Medicine Journal*, vol. 4, no. 1, pp. 51–57, Jan. 2010, doi: [10.2174/1874387001004010051](https://doi.org/10.2174/1874387001004010051).[◦]
- [32] M. D. Harris, M. Datar, R. T. Whitaker, E. R. Jurrus, C. L. Peters, and A. E. Anderson, "Statistical shape modeling of cam femoroacetabular impingement: STATISTICAL SHAPE MODELING OF FAI," *Journal of Orthopaedic Research*, vol. 31, no. 10, pp. 1620–1626, Oct. 2013, doi: [10.1002/jor.22389](https://doi.org/10.1002/jor.22389).[◦]
- [33] L. Ferrarini, H. Olofsen, W. Palm, M. Vanbuchem, J. Reiber, and F. Admiraalbehloul, "GAMES: Growing and adaptive meshes for fully automatic shape modeling and analysis," *Medical Image Analysis*, vol. 11, no. 3, pp. 302–314, Jun. 2007, doi: [10.1016/j.media.2007.03.006](https://doi.org/10.1016/j.media.2007.03.006).[◦]
- [34] M. Frysz, J. Gregory, R. M. Aspdén, L. Paternoster, and J. H. Tobias, "Sex differences in proximal femur shape: findings from a population-based study in adolescents," *Scientific Reports*, vol. 10, no. 1, p. 4612–4613, Mar. 2020, doi: [10.1038/s41598-020-61653-4](https://doi.org/10.1038/s41598-020-61653-4).[◦]
- [35] Martha C. Castaño-Betancourt *et al.*, "The contribution of hip geometry to the prediction of hip osteoarthritis," *Osteoarthritis and Cartilage*, vol. 21, no. 10, pp. 1530–1536, Oct. 2013, doi: [10.1016/j.joca.2013.06.012](https://doi.org/10.1016/j.joca.2013.06.012).[◦]
- [36] A. Murphy, "Hip (AP view)," *Radiopaedia.org*. Radiopaedia.org, Mar. 2018. doi: [10.53347/rID-58728](https://doi.org/10.53347/rID-58728).[◦]



Protocol Proximal Femur SSM points

1.1 Lesser trochanter

Point (28): Where the lesser trochanter starts bending off the shaft distally. If the lesser trochanter is seen behind the shaft, place this point on the cortex of the shaft at the level of this bend. If the lesser trochanter is not visible at all: missing points.

Point (25): Where the lesser trochanter joins the shaft proximally. If the lesser trochanter is seen behind the shaft, place this point on the cortex of the shaft at this level. If the lesser trochanter isn't visible at all: missing points.

Point (26)+(27): Respectively on the lower and upper corners of the lesser trochanter. If there are no clear corners: space them equally between (28) and (25).

1.2 Rest of proximal femur

Point (0) + (1): Respectively across (28) and (25) on the lateral femoral shaft. If (1) would be above (3) this way, place it just under (2).

Point (3): On the lower lateral corner of the greater trochanter.

Point (2): Equally spaced between (1) and (3).

Point (6): On the upper lateral corner of the (anterior) greater trochanter.

Point (4)+(5): Equally spaced between (3) and (6).

Point (7): On the medial upper corner of the anterior greater trochanter. If not visible, equally spaced between (6) and (8).

Point (8): Where the anterior greater trochanter joins the femoral neck (usually at an angle and at a sclerotic corner).

Point (13): On the superolateral side of the femoral head, where the "best fitting circle" around the convexity of the femoral head seems to start. In case of a cam bump, osteophyte, or other irregularity: place (13) right after this bump ends, and the circle begins.

Point (21): On the inferomedial side of the femoral head, where the convexity of the femoral head seems to end. (The neck bends off after this point).

Point (14-20): Equally spaced between (13) and (21), unless there is a clear fovea dip, in which case the adjacent points, usually (18) and (19), are placed just outside of the fovea. Point (17) will be placed halfway across the 'semi'-circle between (13) and (21).

Point (9)+(34)+(10)+(35)+(11)+(36)+(12)+(37)+(38): Equally spaced between (8) and (13). In case of irregularities like a cam bump or osteophyte, follow the outlining contour as closely as possible. Point (39): Equally spaced between (13) and (14).

Point (22): At the deepest point of the inferomedial concavity of the femoral neck, so that (21-25) will follow the medial cortex of the femoral neck as closely as possible.

Point (23)+(24): Equally spaced between (22) and (25), following the medial cortex of the femoral neck.

1.3 Greater trochanter, posterior part

** If the posterior greater trochanter is somehow not visible: (29-34) missing points. Point (30): On the upper medial corner of the posterior greater trochanter.

Point (29): Between (6) and (30), following the contour. If there is a clear angle, put it there.

Point (31): On the medial corner of the posterior greater trochanter, where it starts to drop downwards (caudal). This is independent of the femoral neck, so it can be before or after it dips behind the femoral neck, depending on the rotation of the proximal femur.

Point (32): Where the posterior greater trochanter is dropping straight down, right before it bends medially.

Point (33): On the end of the sclerotic line right after the medial bend, following the contour of the posterior greater trochanter.

1.4 Curve model (with new landmarks incorporated):

Femur curve: 0, 1, 2, 3, 4, 5, 6, 7, 8, 9, 34, 10, 35, 11, 36, 12, 37, 38, 13, 39, 14, 15, 16, 17, 18, 19, 20, 21, 22, 23, 24, 25, 26, 27, 28 Greater trochanter curve: 6, 29, 30, 31, 32, 33

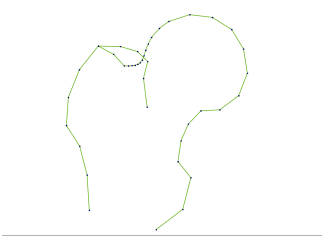
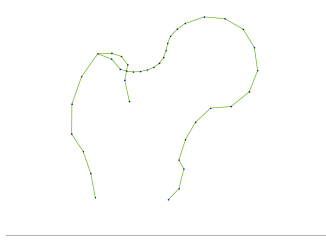
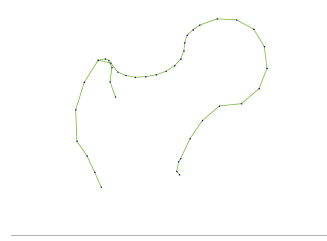
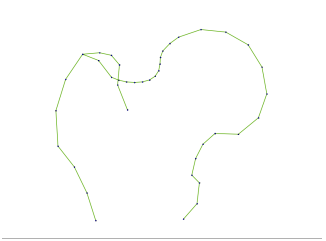
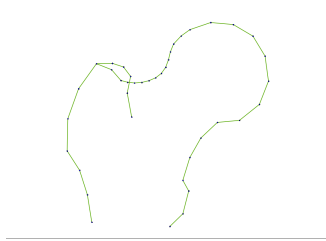
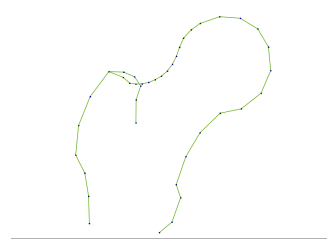
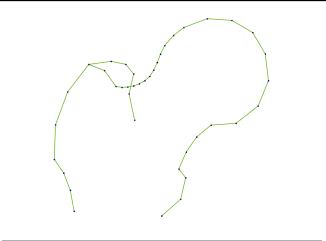
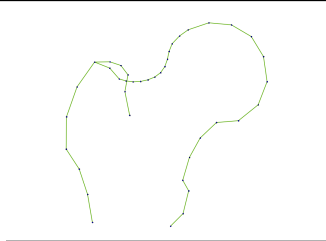
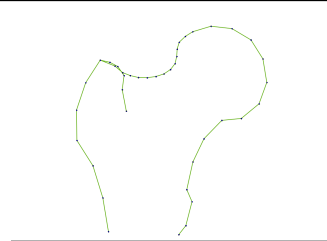
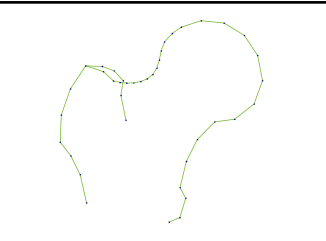
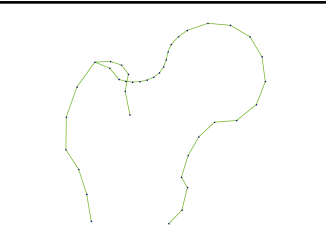
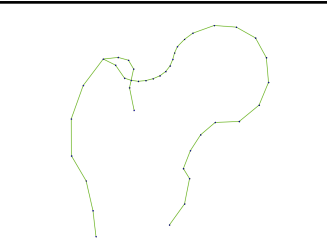
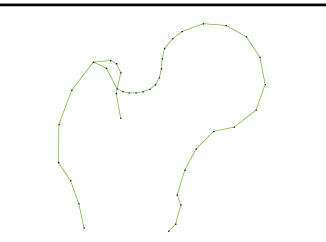
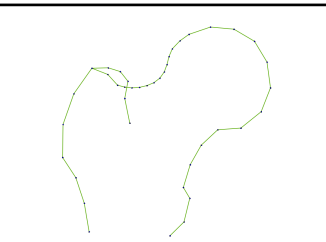
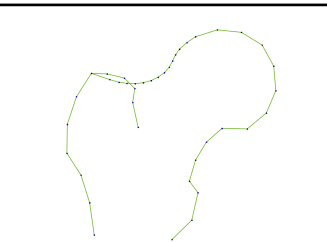
1.5 General rules:

- Osteophytes of the femoral head are included in the model. Follow the outermost contour. We can later correct for these with the radiological assessment data. - Non-identifiable landmarks: missing points (write in separate log file) - Only follow clear bony structures, not projecting shadows. - Every hip is different, so not all anatomical landmarks might be clearly visible in each radiograph. In case of systematic doubt or error: discuss!

B

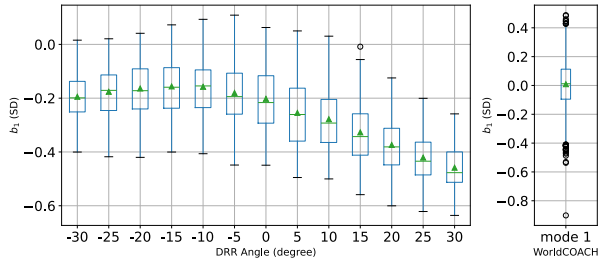
Shape modes of WorldCOACH

Table B.1: Modes of 2D SSM based on WorldCOACH.

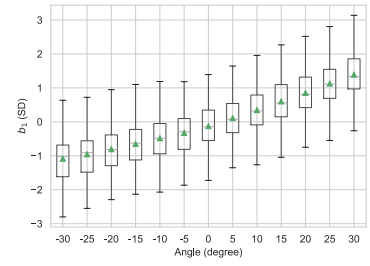
World- COACH and DRR	$-3SD$	Mean	$+3SD$
Mode 1			
Mode 2			
Mode 3			
Mode 4			
Mode 5			

C

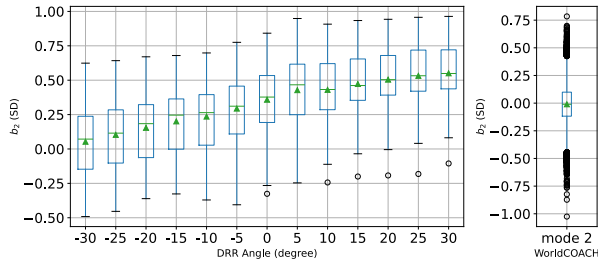
Boxplots: zoomed in



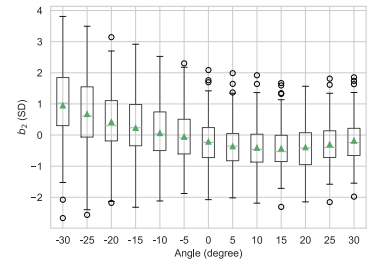
(a) Mode 1, WorldCOACH and DRR.



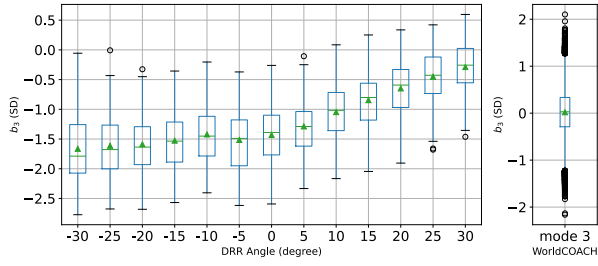
(f) Mode 1, DRR only.



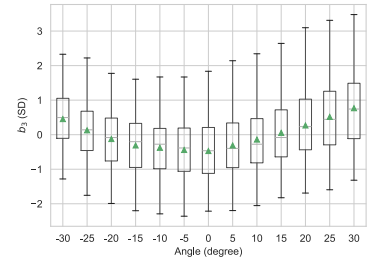
(b) Mode 2, WorldCOACH and DRR.



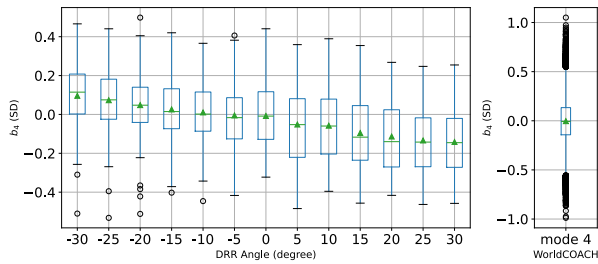
(g) Mode 2, DRR only.



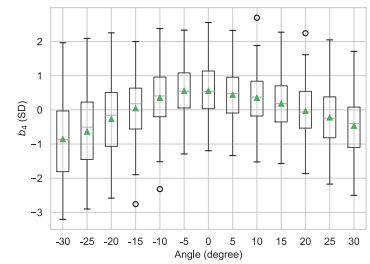
(c) Mode 3, WorldCOACH and DRR.



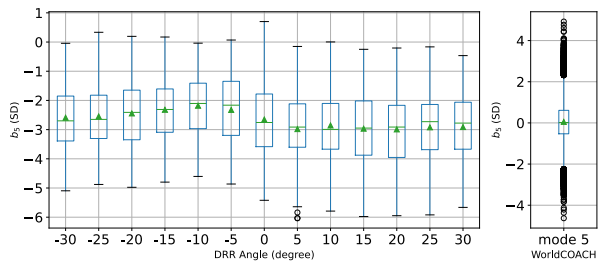
(h) Mode 3, DRR only.



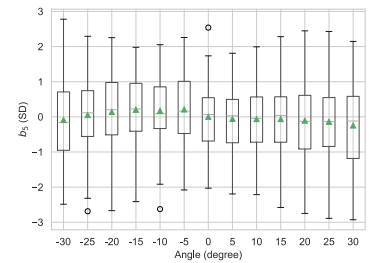
(d) Mode 4, WorldCOACH and DRR.



(i) Mode 4, DRR only.



(e) Mode 5, WorldCOACH and DRR.



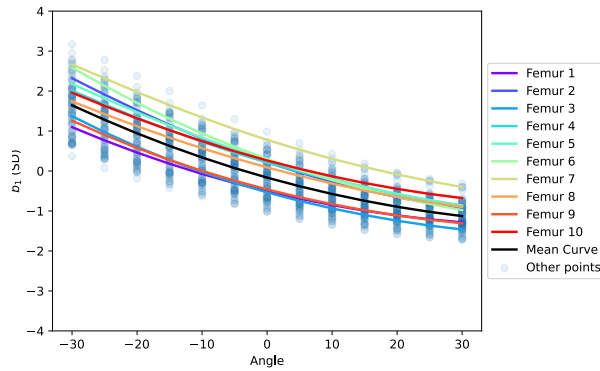
(j) Mode 5, DRR only.

Figure C.1: The zoomed in boxplots of Figure 3.15

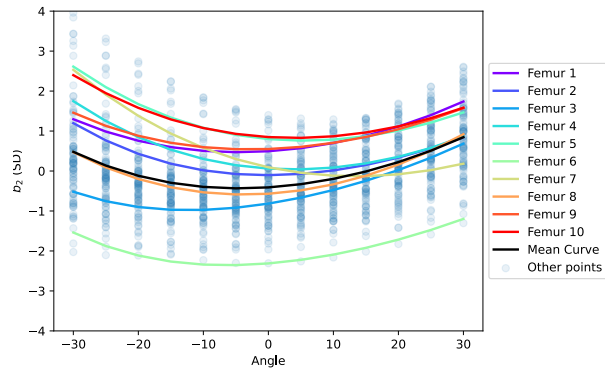
D

Curves of tracked bones in Projected 2D

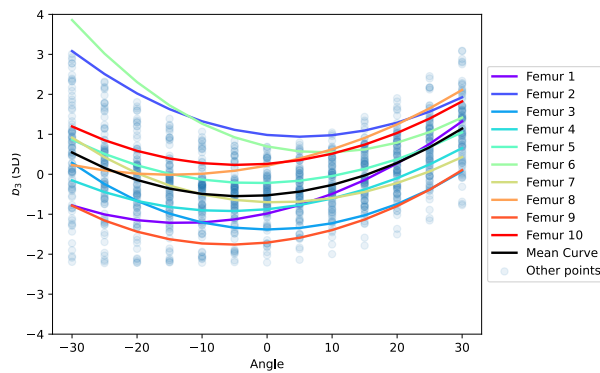
SSM



(a) Mode 1, Projection SSM

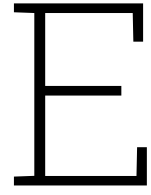


(b) Mode 2, Projection SSM



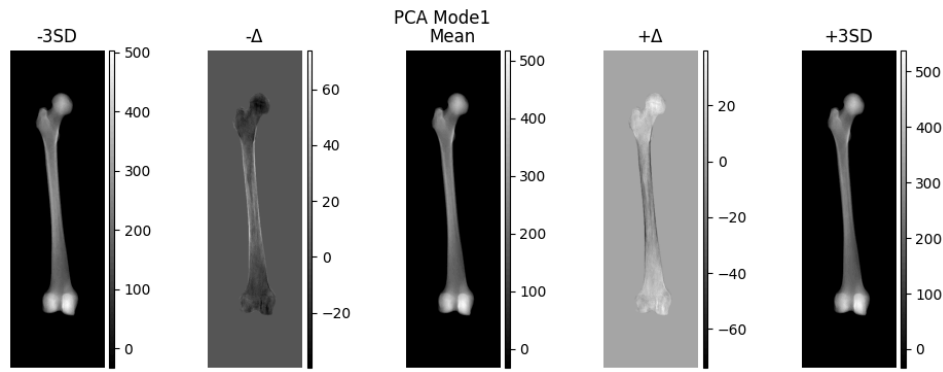
(c) Mode 3, Projection SSM

Figure D.1: Shape variation of different modes and the b values of the a separate SSM not mentioned in the rest of the thesis. This SSM is based on the key landmark points described in Section 2.3.2.4, when projected in different directions like a DRR model.

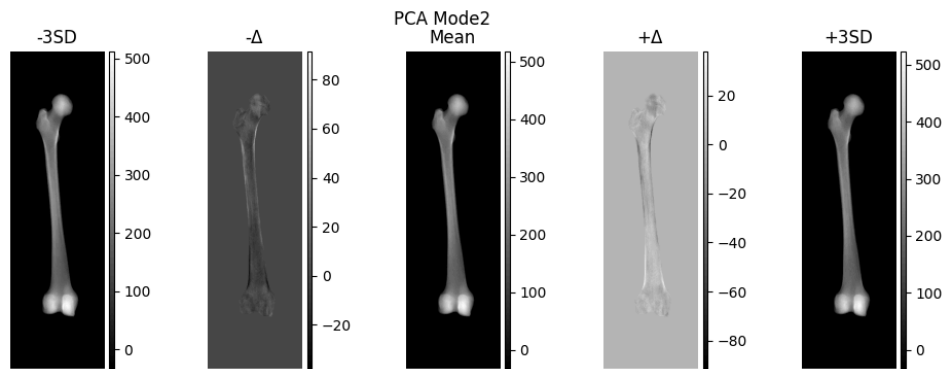


Statistical Appearance models

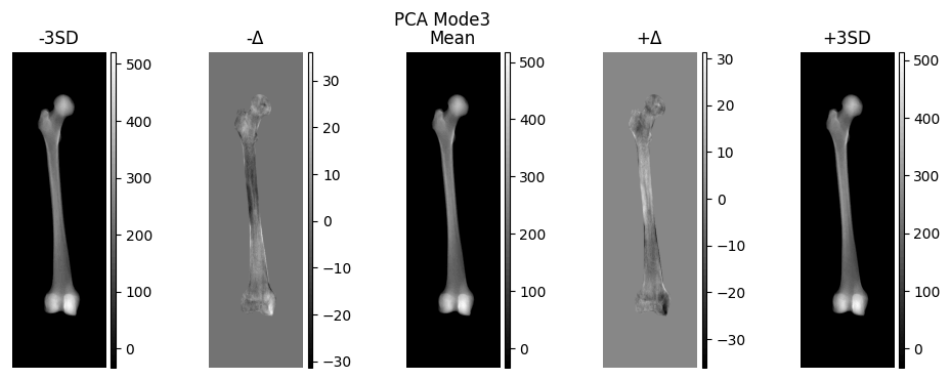
PCA can also be applied to the voxel intensity of a CT. Instead of shape analysis, the bone density differences can be analysed, this is called a statistical appearance model (SAM). The varying brightness represents the variation in bone density corrected for the same shape. This is done by freezing the bone shape to a mean shape and letting the principal component vectors represent the intensity of each pixel or voxel. Due to the calculations with a lot of large matrices (every pixel is represented with a number), this is very intensive to calculate, therefore a model is created using 29 (instead of 99) bones from the APPROACH dataset.



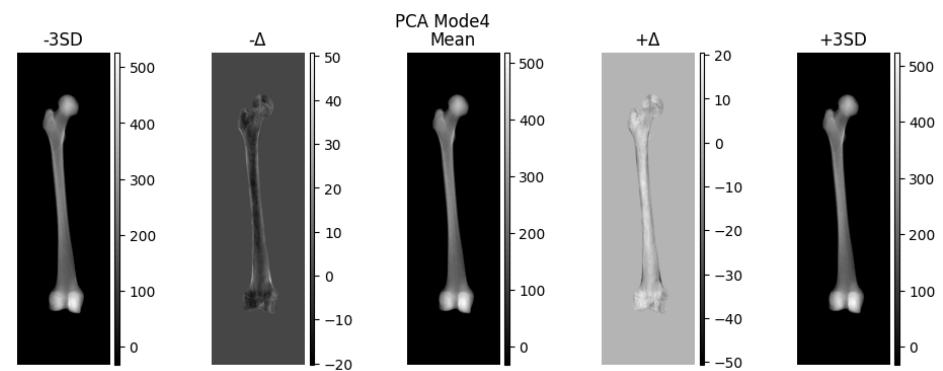
(a) Mode 1, SAM



(b) Mode 2, SAM



(c) Mode 3, SAM



(d) Mode 4, SAM

Figure E.1: Bone intensity variation across a population.